AAPG BULLETIN

Stratigraphy, facies and evolution of deep-water lobe complexes within a salt-controlled intra-slope mini-basin

Gemma Doughty-Jones, Mike Mayall and Lidia Lonergan

AAPG Bulletin published online February 15, 2017
doi: 10.1306/01111716046

Cite as: Doughty-Jones, G., M. Mayall and L. Lonergan , Stratigraphy, facies and evolution of deep-water lobe complexes within a salt-controlled intra-slope mini-basin, *(in press; preliminary version published online Ahead of Print* February 15, 2017*):* AAPG Bulletin, doi: 10.1306/01111716046.

Stratigraphy, facies and evolution of deep-water lobe complexes within a salt-controlled intra-slope minibasin

Gemma Doughty-Jones*, Mike Mayall and Lidia Lonergan

Department of Earth Science and Engineering, Imperial College London, South Kensington Campus London SW7 2AZ

* now at BP, Chertsey Road, Sunbury-on -Thames, Middlesex, TW16 7BP

Revised for AAPG BULLETIN 24 November 2016

ACKNOWLEDGEMENTS

GDJ was funded by a NERC-CASE award with BP (NE/H017682/1). We thank BP, Sonangol, Statoil and SSI for allowing us access to the seismic and well data required for this research and for permission to publish. Steve Dee is thanked for both logistical and scientific support during the project. We thank P.A. Allen and P.W. Haughton for their comments on an early version of this paper.

ABSTRACT

A succession of four deep-water lobe complexes deposited within a salt-controlled minibasin have been imaged in unprecedented detail on high resolution, high frequency 3D seismic reflection data. The ponded interval was deposited over approximately 2.7 m.y. and consists of four discrete sequences, each of which contains one lobe complex. There is a systematic change in the shape and orientation of the lobe complexes through time: the two older lobe complexes are oriented broadly north-south and are up to 10 km (6.2 mi) long by 5 km (3.1

mi) wide, whereas the youngest lobe complexes are oriented southeast-northwest and have a rounder shape (9 km (5.6 mi) long by 8 km (5 mi) wide). The north to south migration of the feeder channel entry point and the change in lobe complex orientation is attributed to growth of the basin-bounding salt structures.

Each lobe complex is composed of a feeder channel, multiple individual lobes formed of a trunk channel and a diverging network of smaller distributary channels, commonly fringed by a high amplitude band. The lobes are on average 1.6 km (1 mi) long by 1.3 km (0.8 mi) wide and are fed by trunk channels that range from 60 m (197 ft) to 200 m (656 ft) wide, with thicknesses up to 15 m (49 ft). Variation in lobe shape and spatial location is driven by the response of the lobes to topographic growth along the edge of the basin and as well as inherited seabed relief generated by previous lobe growth. In areas where lobe development is constrained by structural growth along the edge of the basin the lobes become elongated and divert away from the growing topography.

Lobe complexes of similar scales have been described in detail in outcrops and in unconfined settings on the seafloor but this is the first study to describe these systems in such detail in the subsurface, resolving the individual lobes and lobe elements within a ponded intra-slope basin The high resolution plan-view images help bridge the gap between the fine-scale sedimentological studies that have been carried out on lobe complexes and sheet sands in outcrop for the past twenty years with more recent research on less well-resolved seismically imaged systems.

The sheet sands described in outcrop studies can be correlated with features seen in the plan-view amplitude extraction maps: we record densely channelized lobes passing laterally into more branched, thinner channels and lobe elements then terminating in a high amplitude fringe. We relate these seismic characteristics to outcrop facies of channnelised, amalgamated and layered sheets.

INTRODUCTION

Lobe complexes form at the termination of deep-water submarine channel systems, down-dip of submarine feeder conduits that can include short-lived gullies to long-lived leveed fan valleys, submarine channel mouths or 'transition points' (Posamentier and Kolla, 2003, Posamentier and Walker, 2006, Deptuck et al., 2008). Such systems were originally thought to consist of flat-layered deposits (sheet sands) resulting from rapid suspension fallout due to depletion at the termination of channel-levee systems (Normark, 1970, Mutti and Normark, 1991). However, more recent studies have revealed that they are comprised of extensively channelised sandy depositional bodies most commonly termed lobes (Nelson, 1992, Twichell et al., 1992, Piper et al., 1999, Adeogba, 2005, Gervais et al., 2006, Saller, 2008, Prélat et al., 2009, Prélat et al., 2010). Many studies have also looked specifically at fans that form in ponded settings, particularly those located in the Gulf of Mexico (Winker, 1996, Beaubouef and Friedmann, 2000, Steffens et al., 2003, Al Ja'Aidi et al., 2004, Adeogba, 2005, Covault and Romans, 2009b, Gamberi and Rovere, 2011, Prather et al., 2012, Oluboyo et al. 2014, Damuth and Olsen 2016). Building on this body of work Gamberi and Rovere (2011) define four types of submarine fan system: basin plain fans, transient fans, terminal fans and ponded fans. Those discussed in this paper fall within the ponded and transient lobe categories.

Ponded lobe complexes commonly occur in confined basin settings where complex seafloor has been generated, for example by active faulting or the diapiric movement of salt and/or mud (Ori and Friend, 1984, Brunt et al., 2004, Gamberi and Rovere, 2011, Jones et al., 2012). This topography generates depressions on the seafloor that have the potential to act as confining basins trapping all, or a proportion of the sediment that enters the basin until the negative topography is eliminated.

The study area for this paper is located within a minibasin in the Lower Congo Basin approximately 200 km (124 mi) offshore northern Angola on the continental slope (Figure 1). The stratigraphic interval of interest comprises ponded fan lobe complexes that developed between 8.3 Ma and 5.6 Ma (Figure 2). By imaging a series of lobe complexes fully, the work presented here builds on previous studies through its use of a high-resolution 3D seismic dataset. The resolution of the data allows the stratigraphy and internal geometries to be imaged in unique and exceptional detail, thus bridging the gap between outcrop data and conventional resolution seismic data in a novel way. The lobe complexes investigated are all contained within one structurally controlled minibasin, and hence this work focuses on the characteristics and evolution of lobe complexes within a ponded setting. The lobe complexes were deposited in the minibasin during a reduction in the shortening rate, and infilled the topography generated from the earlier period of growth on the surrounding salt walls and salt-cored folds (Jones et al., 2012).

DATA AND METHODOLOGY

A high-resolution, and high frequency, 3D seismic reflection dataset covering approximately 1,400 km^2 $^{(}$540 $miles^{2)}$ was used throughout. It has an inline and crossline spacing of 6.25 m (20.5 ft) and a vertical sample rate of 2 ms twtt, instead of the more usual 4 ms sample rate used for 'standard' 3D surveys. The frequency content of the dataset averages 70 Hz giving a vertical resolution of 6-10 m (19.6-33 ft) within the ponded lobe complex interval. Detailed seismic mapping of the dataset identified four sequences within the ponded package based on stratigraphic relationships, seismic character and depositional events. The stratigraphy within these sequences has been isoproportionally sliced to mimic the topography of the basin with maximum thicknesses of 25 ms twtt towards the centre. A root-mean-squared (RMS) amplitude extraction has been applied to each interval, calculating the square root of the sum of the squared amplitudes divided by the number of samples taken within the window. This means that the both maximum positive and negative amplitude values are highlighted, increasing the amount of information extracted from the dataset. The channels that are clearly imaged on amplitude maps (Figure 3B) are considerably more cryptic on vertical seismic lines. They appear as subtle convex-up and/or brighter amplitudes (Figure 3C). The consistency and continuity of the trunk and distributary channels on the maps give us confidence that these are real geological features.

There are no wells that penetrate this sequence to provide lithological control. However there are wells near-by with high-resolution nannofossil and foraminiferal biostratigraphic data that can be correlated into this area. The biostratigraphic data has been tied to absolute time scales that provides age dates for the mapped horizons.

In this paper, the terminology used by Prélat et al. (2009) in the Karoo Basin, South Africa is applied; lobe elements, lobes and lobe complexes are all recognised in seismic amplitude extractions (Figure 3). Each lobe complex is fed by a single feeder channel that can be imaged within the minibasin in some sequences, but in others it has been disrupted by later salt diapirism and lies outside the well-imaged area (Figure 3B). The feeder channel branches to form smaller trunk channels. These are imaged in all sequences and often in great detail ranging in width from 60–200 m (197-656 ft). The trunk channels (abbreviated to ‘channels’ in this paper) end with a series of finer branching distributary channels with widths of 30 m or less. There is often an area of smoother bright amplitude associated with the finer branching, beyond and between the channels. The association of the finely branched channels and the area of smoother amplitude are interpreted as the lobe (see x and y in Figure 3B). The lobes are on average 1.6 km (1 mi)long by 1.3 km (0.8 mi) wide. Within the lobes smaller clusters of splayed channels are interpreted as potential lobe elements. Lobes stack by spatially shifting to form discrete lobe complexes (Figure 3A and B).

The channels have been mapped on the RMS map of each isoproportional interval (Figure 3B). The channel outlines for each interval within a sequence have been overlain to show the progradation, retreat or lateral shifting of the lobe systems with time. The maps from the upper three sequences have very high resolution and each interval is described and interpreted in detail. The lower sequence maps have poorer resolution and are more difficult to interpret. However we have confidence in the interpretations from the details that can be seen in the upper sequences. For the lower sequences we show only some of the intervals to illustrate the main movement of the lobe systems. The widths of the channels have been measured at several points along their length and these data are presented as histograms for each sequence.

Local mass transport complex (MTC) deposits are also visible within some of the ponded intervals, particularly along the margins of the basin. These have been identified with a slightly dim, chaotic seismic signature in cross-section (Figure 4A) and a generally low-amplitude disorganised, blotchy seismic signature in the amplitude extraction maps. In many cases this facies is thin and difficult to recognise on seismic lines but is clear on amplitude extraction maps. In these cases it is difficult to ascertain the age relationship between the MTC and the surrounding lobes, and to deduce whether the MTC has eroded any underlying channel-lobe stratigraphy, or has caused topography to which the channel systems have reacted.

STRUCTURAL SETTING

The ponded deposits studied here are located approximately 200 kms (124 mi) from the upper Miocene shelf edge and are bounded on all sides by salt-related structures (Figures 1 and 2).

The major boundary that prevents sediments exiting the minibasin lies on the western side of the minibasin where a long-lived salt wall prevents sediment flow down the slope and out into the basin (Figure 1, Areas B, D and E). A series of linked salt-cored anticlines in Area C further constrain the north-western boundary. These linked structures show increased movement before deposition of the ponded lobe complex sediments resulting in the generation of significant bathymetric relief. However, analysis shows that growth of relief had slowed when the ponded sediments were deposited resulting in a period of relative structural quiescence (Jones et al., 2012). Subsequently more detailed analysis of the system suggests that although the basin was largely passively infilling, there were also periods of some subtle but important structural development of sea-floor topography. The eastern boundary, (Area F in Figure 3), is formed by a salt-cored anticline which has been pierced by a salt diapir after the formation of the ponded interval. The development of the associated salt canopy post 5 Ma, has obscured the imaging of channels feeding from the east within the ponded section.

A northeast-southwest trending arcuate normal fault has exerted control on the thickness of the ponded sediment during its deposition (Figure 1). Growth of the fault is likely to be linked to the salt structure beneath it, forming due to collapse related to salt withdrawal and/or lateral flow into the larger salt structure at its south-western end (Figures 1 and 5). The fault was active during the ponded interval, but also later as it offsets strata younger than 5.6 Ma, consistent with a salt-related origin (Figure 5E). The two youngest ponded sequences extend south of this fault. A few local MTC deposits occur before, during and after the deposition of the ponded lobe complexes and are largely sourced from the western salt-cored anticline (Area C) and the salt structure within Area F on the eastern boundary of the minibasin.

STRATIGRAPHIC FRAMEWORK

Ponded sediments occur primarily between 9.7 Ma and 5.6 Ma (H90 and H110). Within this period two packages of ponded sediments were deposited (Figure 4); the oldest between 9.7 Ma and 8.3 Ma and the younger between 8.3 Ma and 5.6 Ma. The deposition of a unit of laterally extensive, parallel, low-amplitude layered reflections between the two ponded intervals suggests a hiatus in sediment input to the area with only background mudstones deposited (Figure 4). Here we analyse the younger of the two ponded packages in detail. Within this interval five sequence boundaries have been recognised and mapped; P10 (oldest) to P50 (youngest) (Figure 4). The younger ponded package has a time span of 2.7 Ma, implying that each of the constituent four sequences could have a duration of approximately 0.7 Ma. The intervals contained within these stratigraphic boundaries are analysed in detail and their seismic stratigraphic characteristics are discussed in the following paragraphs.

Cross-sections through the basin and isopach maps show how the package thicknesses vary through time (Figures 4 and 5). The position of the edges of the lobe complexes in the isopach maps are in part a result of the resolution of the data. A thinner sequence below resolution of the seismic i.e. 6-10 m, may extend further into the basin. In the earliest phases (P10 – P30) a thicker sediment package is deposited towards the north of the basin, whereas in the P30 – P50 intervals the thickest sediment packages are deposited towards the south of the area. All the packages appear to thin towards the western edge of the basin with all but the interval between P40 to P50 also thinning towards the east. All sequences are eroded in the north of the basin by a younger channel (Figure 4B).

P10-P20

This unit consists of fairly continuous horizons that appear to thin towards the confining edges of the basin, onlapping in the west and onto the topographic high located towards the north of the area (Figure 4).

P20-P30

There is clear onlap of reflections onto the P20 surface, mainly within the centre of the interval and away from the edge of the basin (Figure 4A). In the west the reflections extend a large distance up the edge of the anticline within Area C onlapping onto, and ending against, it (Figure 4A). The terminations in the east are complicated by the presence of a coeval MTC with individual horizons within the interval lapping against it. The P30 horizon can be traced across the basin, clearly onlapping the structures on eastern, western and southern sides, and also blanketing the older MTC in the east (Figure 4A).

P30-P40.

The P30 and P40 horizons are strong, high-amplitude, continuous reflections that extend across the basin bracketing a package consisting of highly continuous bright reflections. The reflections within this package onlap against the structure to the east but thin and continue over the western structure. The package thins towards the north and thickens to the south (Figure 4B). P30 and P40 horizons can both be traced south of the normal fault where the P30 horizon becomes the base of the ponded package. The P30 horizon is offset by an average of approximately 50 m and the P30 to P40 interval is almost twice as thick south of the normal fault, showing that it was active during the deposition of this interval (Figure 5C, E).

P40 – P50.

This is the thinnest of the mapped packages and has a very similar distribution to the P30-P40 unit with the beds onlapping the structure on the eastern margin of the basin. The interval continues up the flanks of the anticline to the west, almost reaching the crest and thinning significantly as it does so (Figure 4A). Overall the P40 – P50 interval comprises high-amplitude, discontinuous reflections that thin towards the north and are cut by the normal fault to the south (Figure 5D). Although the P40 and P50 horizons are offset by the fault there was little measurable growth across it at this stage (Figure 5D).

As described and illustrated in Figure 5, the thickness of the units within the ponded interval varies through time. Assuming that the thickest part of the sedimentary packages correlates with the main sediment input point to the basin, Figure 5 illustrates a gradual change from sediment entering primarily from the north of the area during the P10 – P20 unit to sediment entering the basin from the east and further south within the area in the P40 – P50 interval. The P30 – P40 unit is particularly interesting as the sediment enters the basin through an area that has an active salt body at the present day. This suggests that this salt structure was probably not active at the time of sediment deposition. The normal fault that separates the north and south of the basin affects the sediment distribution from P30 to P40 times (ure 5E). During P10-P30 times the sediment packages thin towards the normal fault and terminate to the north of it (Figure 5 A, B, E). This thinning could indicate the start of fault movement before, or during, this time window, where movement on the fault caused rotation and tilting of the footwall to the northeast, generating a relative topographic high along the length of the footwall. During both P30-P40 and P40-P50 times the thickest sediment is deposited in the southeast of the basin, directly to the south of the normal fault, suggesting that both units may have sourced by a similar sediment feeder system (Figure 5 C, D), as is borne out by the amplitude analysis (see discussion below).

LOBE COMPLEX FACIES AND ARCHITECTURE

P10 – P20

The P10 – P20 unit is the oldest package within the ponded section. The deposit thins from 90 m in the north towards the southeast, east and west of the basin (Figure 5A) confined in extent by the highs formed by the salt structures on the eastern and western sides of the basin. The sequence is also cut by a younger northeast-southwest trending erosional channel system in the north (Figure 4B).

Four isoproportional amplitude extractions through the interval show that the sediment entering the basin during this period was comprised of narrow, high amplitude channels. The image resolution is poor in some of these intervals and a couple have been selected to show the main features of this sequence. During the oldest interval the channels entered the basin from an entry point to the north-northeast (Figure 6A, B). Dispersed, small channels up to 25 m (82 ft) in width which branch frequently, and which can be traced up to 6 km (3.7 mi) into the minibasin form most of this interval. The majority of the channels are oriented northeast-southwest, with a mean flow direction of 038-212 ±7°; there is also a minor a cluster of channels in the northwest corner indicating flow in a more east-westerly direction.

As the system becomes younger it covers less area in the basin with the maximum deposition point retreating closer to the sediment entry point in the north (Figure 6B). Interval 3 contains significantly fewer channels than the previous interval with a cluster of more northeast-southwest trending channels in the north of the area extending approximately 3 km (1.9 mi) into the basin (Figure 6B). Both intervals show an association of small branching channels and smoother bright amplitudes interpreted as a series of lobes. The main flow orientation remains NE-SW (Table 1)

P20 – P30

Within the P20 – P30 unit the thickest sediment package is deposited in the east of the basin within an 80 m thick depocentre (Figure 5B). The overall depositional thickness of the sediment is controlled by the entry point and the underlying package, the P10 – P20 unit, with the P20 – P30 unit thinning on either side of the main P10 – P20 depocentre (Figure 5A, B). Onlap of individual events within the P20 – P30 interval can be observed on the margins of the thickest part of the P10 – P20 unit (Figure 4A), indicating that the underlying P10 – P20 package formed depositional relief within the basin during P20 – P30 times and influenced the position of flows entering the basin. The strata also onlap an area of MTC's in the eastern side of the basin (Figures 4A, 7).

Four isoproportional RMS amplitude extraction maps through the P20 – P30 unit reveal details of the trunk, distributary channels and lobes that form this package (Figure 7). The input of the lobe complex is from the northeast with channels predominantly oriented northeast-southwest across the basin, with little significant variation between intervals, except for interval 4 where a more E-W trend is developed along the northern side of the basin (see rose diagrams on Figure 7; Table 1). The main feeder channel is only imaged in the youngest interval (Figure 7D) when the system has prograded into the basin. In the older intervals the feeder channel is probably eroded by the E-W trending younger channel to the north.. The RMS amplitude maps and the channel composite maps (Figures 7 and 8) show progressive progradation of the lobe complex into the basin through the entire sequence. This is particularly well demonstrated between intervals 2 and 3 (Figure 8B). The most westerly extending channels deposit lobes against the western margin of the basin. There is well-defined lateral compensational stacking with younger channels occupying the areas between preceding older channels and again this is evident between intervals 2 and 3 and then again between 3 and 4 (Figure 7 B,C and Figure 8 B,C). We note that although the majority of the distributary channels and associated lobes move laterally through time, a north-south oriented channel system remains fixed through the sequence with little lateral movement on the eastern margin of the basin. Channel widths range from 30-300 m (98-964 ft) with an average of width of c.100m±50m (326±164 ft)(Figure 9A; Table 1).

Multiple branching of small channels, indicating the development of lobes, is imaged to some extent in all sequences but is best seen in intervals 3 and 4 (Figure 7 C,D). Smooth areas of bright amplitude are often associated with the channelized lobes particularly in the south of the basin in intervals 2 and 3 and the western part of the basin in intervals 3 and 4 (Figure 7C d). The areas of the lobes range in size from 1.7 km^2 (0.66 mi) to over 5 km^2(1.9 mi). On the eastern side of the basin a large mass transport complex controls the distribution of the lobe complex (Figure 4A).

P30 – P40

The isopach of this sequence illustrates significant changes from the underlying sequences (Figure 5). The thickest part of the sequence, up to 80 m (262 ft), occurs in the southeast of the minibasin with thinning to the north, west and southwest. For the first time a sequence extends south of the normal fault where a thick P30-P40 interval has accumulated, however for this paper we focus mainly on the area north of the fault.

The P30 – P40 sequence has been sub-divided into six intervals. The oldest two intervals are dominated by MTC deposits that extend throughout the basin. This might suggest there was some structurally activity between the deposition of the P20 – P30 and the P30 – P40 sequences which sourced debris flows and/or slumps. Alternatively the MTC deposits may have formed from structures that were exposed in the basin during a period of relative sedimentary quiescence. A large MTC deposit is also present in the southeast of the basin visible within intervals 4, 5 and 6 in particular (Figure 10) but it is challenging to discern any age relationship to the lobes with confidence. The MTCs may be older than the lobes and onlapped by them or younger and be cutting through them.

The input of the lobe complexes has now switched to the southeast (Figure 10) and the channels correspondingly flow from SE to NW across the basin with vector means ranging from 307-316° (Table 1). The channels cannot be imaged under the salt diapir canopy (Figure 10) but projection of their orientation suggests that they could be originating from a common feeder channel located at least 1-2 km (0.6-1.2 mi) to the east of the map, under the salt canopy on the SE margin of the basin.

The initial development of the lobe complex (interval 3; Figure 10A) suggests that the depositional system filled most of the basin and extended to its western margin. Through the subsequent intervals (Figure10 B, C) the complex retreated eastwards a distance of ca. 3 km (1.86 mi) from the distal limit reached on the western margin of the basin during interval 3. The final interval shows renewed progradation of the complex into the basin (Figure 10D). The composite maps of the channels (Figure 11) illustrate this pattern of lobe movement very clearly. They also show well-developed compensational stacking as younger channels relocated to areas between older systems.

Lobes are well-developed at the end of the distributary channels in all sequences. Multiple small branching channels associated with smoother areas of generally brighter amplitudes are well-imaged. Channel widths vary from over 200 m (656 ft) to less than 60 m (197 ft) with an average width of between 96m (315 ft) and 109 m (358 ft) (Figure 9B; Table 1).

P40– P50

The P40 – P50 unit is the youngest within the ponded sediment package and like the previous P30-P40 interval it extends south of the normal fault. It reaches a maximum thickness of 75 m (246 ft)on the footwall side of the fault and has a locally thick depocentre immediately south of the fault (Figure 5D). The isopach thickness map shows that the thickest sediment volume was deposited in an east-west oriented ‘fan’ shape to the north of the fault and then in a N-S oriented corridor south of the fault (Figure 5D).

North of the fault the main input is again from the southeast. In the youngest two intervals of the unit the channels converge over a wide area towards diapir F (Figure 12 A,B). Their orientation suggests that the feeder channel would be located under the present day diapir canopy. In the upper two intervals a feeder channel can be imaged on the SW side of the diapir (Figure 12 C,D).

North of the fault the channels broadly radiate out across the basin with mean flow directions from SE to NW for all intervals (Table 1). The first channels (Figure 12A) extend across the basin to the western margin and through the whole sequence there is very little evidence for progradation or retreat of the system. However the orientation and density of the channels does vary through time (Figure 13). In interval 1 there are a number of prominent channels ending in well-defined lobes that have a range of orientations from north-south to east-west and southwest (Figure 12A). An area of mass transport complex is identified from the amplitude map in the east of the basin. The channels and lobes in interval 2 are in a similar location but there is a greater density of smaller channels.

Interval 3 shows a similar range of orientations and channel density but also has a number of good examples of compensation stacking as the channel and lobes are offset from the interval 2 system. Interval 4, the shallowest interval, has well-imaged channels and lobes. The input point is focused to one feeder channel that can be seen southwest of diapir F. The channels have a similar range of orientations to the underlying sequences but have a more north-south trend in the north and east of the basin (Figure 12D, 13). This interval again shows compensation stacking when compared to the location of channels and lobes in interval 3. The channels range in width from 45 (148 ft) to 265 m (869ft). There are a greater number of narrower channels between 45 (148 ft)_ and 75 m (246 ft)in width in interval 2; interval 4 has the greatest range of channel widths. However we note that there is very little difference between the mean widths for these two intervals (Figure 9C, Table 1).

Additionally a very dense network of channels is imaged south of the fault. The channels in intervals 1 and 2 are located approximately 1 km (0.6 mi) from the fault (Figure 12 A,B) while the interval 3 channels are deposited adjacent to the fault footwall spreading out from the input point (Figure 12C). In interval 4 the channels become more widespread and cover an area extending up to 3 km (1.9 mi) from the fault (Figure 12D). The channels are aligned mostly parallel to the fault, responding to the accommodation space forming in the fault hanging-wall.

EVOLUTION OF THE LOBE COMPLEXES´´

The example presented here demonstrates the complete history of the facies and geometries in a ponded lobe complex. Figure 14 presents a summary of the development of the lobe complexes in terms of the extra-basinal and inter-basinal controls and the changing distribution of the main lobe complex elements – feeder, trunk and distributary channels, lobes and MTC's.

P10-P20 (Figure 14A). In this sequence the input point was from the northeast. The facies comprise short preserved lengths of trunk channels terminating in lobes with distributary channels and high amplitude fringes. The feeder channel must have been further to the northeast but has been eroded by a younger channel. After initial progradation, the lobe complex stepped backwards through the sequence.

P20-30 (Figure 14B). The input point was still from the northeast and the sequence shows intra-basinal controls by thinning over the earlier P10-20 sequence, terminating against a MTC in the east, strong north-south alignment of channels and lobes in the east of the basin and onlap against the footwall of an intra-basinal fault. The complex was dominated by trunk channels and lobes which prograded through the sequence and show well-developed lobe switching. In the older intervals the feeder channel is eroded by a younger channel but prograded into the basin by the end of the sequence.

P30-40 (Figure 14C). The input point switched to the southeast because of extra-basinal controls, probably related to movement of the salt diapir. Trunk channels and lobes are well imaged and show many examples of offset compensation stacking. The initial complex extended across the whole basin and then retreated before a final phase of progradation. The intra-basinal fault was active and a thick interval was deposited on the down-thrown side.

P40-50 (Figure 14D). Sediment continued to be supplied from the southeast. In the first phase of progradation the lobe complex extended across the entire basin. Subsequently there was no major advance or retreat of the lobe complex but there are many examples of offset compensational stacking of individual lobes. The extensional fault was active and a dense network of trunk channels formed in the hanging wall of the fault.

Lobe complexes are important reservoirs in many slope systems. At a seismic scale the lobe complexes are broadly sheet-like i.e. they are much wider (km’s-tens of km’s) than they are thick (typically a few tens of metres). Within these broad sheet geometries outcrop and subsurface studies have shown that there are a repeated series of facies and reservoir architectures which will have a strong influence on fluid flow in a hydrocarbon field. The general facies definitions of channnelized sheets, amalgamated sheets and layered sheets (e.g. Sullivan et al., 2000, 2004) provides an excellent framework for describing the reservoir heterogeneity patterns. The Angola example described here builds on this framework by providing some important analogue information through the well-imaged planform data, listed here:

- The trunk channel dominated part of the lobe complexes clearly demonstrates the strong gross permeabilty anisotropy that can be expected in this part of the system.

- The distributive channels and associated non-channelized areas indicate a more areally homogenous reservoir but comparison with outcrops suggests a more complex patern of vertical shale barriers and baffles.

- The maps provide important quantitative data on channel and seandbody geometry dimensions.

- The lobe complexes which show prograding, retreating and compensation off-set stacking patterns demonstrate how vertical stacking of facies with different reservoir properties is generated.

CONTROLS ON LOBE MORPHOLOGY

Overall four stratigraphically distinct phases of lobe complex formation have been recognised within the Angolan ponded sequence studied. Each unit contains a single long-lived lobe complex, one feeder channel branching into several channels and terminates in a series of lobes. However, the orientation of the lobe complexes and the geomorphological characteristics of the channels and lobes that form the lobe complexes vary between the intervals. There are two drivers for changes in the characteristics of the lobe complexes within the basin, allogenic controls including local structural controls and autocyclic sedimentological factors.

Salt diapirism and fault movement within the basin are the structural controls. For example the shift in the feeder channel entry point from the northeast to the southwest between the P20 - P30 and the P30 – P40 units (Figure 5) is likely to have been caused by changes in the feeder channel pathway prior to its entry into the basin. This could either have been driven by structural change (e.g. growth of a salt body up-dip of the basin) or alternatively a stratigraphic change (e.g. avulsion of the channel before entry into the basin). However given the nature of the salt growth in this area, it is most likely that the channel was forced to switch pathways by the growth the salt either on the eastern margin of the minibasin or up-slope further to the east. The orientation of the channels within interval 4 of the P20 – P30 unit (Figure 7 D), the interval directly before the switch in sediment entry point, is much more varied than those in the previous intervals with a slightly more east-west orientation overall. This could indicate that even by this stage the channels are responding to changes in the salt structures to the east of the minibasin, thus suggesting a structural driver to the main switch in orientation.

The normal fault that divides the minibasin in two has exerted varying degrees of control on the sediment distribution throughout the entire interval of lobe complex development. It is possible that subtle fault movement during the deposition of the P10 - P20 and P20 – P30 units, when sediment input was from the north (Figures 6,7), caused uplift and rotational tilting of the footwall creating a topographic high on the southern margin of the basin next to the fault. This high may have prevented sediment from being deposited any further south and be responsible for the slight western bend observed in the channels deposited in the southern half of the basin during the P20 – P30 interval (Figure 7). The fault has a more obvious direct control on the sediment distributed within the basin during the P40 – P50 interval with clear variation in the characteristics and distribution of the channels deposited both to the north and south of the fault (Figures 12,13). The throw of the fault decreases as the system becomes younger allowing the channels to flow across the eastern tip of the fault as the system progrades into the basin (Figures 12 and 13).

Autocyclic sedimentological controls work at a range of scales from lobe complex to individual lobes. There are changes in the distribution of the sediments deposited within the lobe complexes that appear to be a direct response to topographic change within the basin. This is particularly apparent between the P10 – P20 unit and the P20 – P30 unit: isopach analysis of the P10 -P20 unit shows that there is a thick wedge of sediment in the north of the basin, corresponding to the area surrounding the feeder channel, whereas in the following unit, P20 – P30, the thickest sediment was deposited on either side of this relative high (Figure 5 A,B). The oldest channels that develop within the lobe complex during the P20 – P30 unit (i.e. those in intervals 1 and 2) respond to the presence of this relative topographic high with the majority clustering down the eastern side of the basin (Figure 7 A,B). The younger feeder channels within this unit (i.e. those imaged in P20 – P30 intervals 3 and 4) are still located mostly to the east of the underlying high, but trunk channels branch away from these ending in lobes towards the western edge of the minibasin. This implies that by the time intervals 3 and 4 were deposited the topographical lows had been filled by sediment from intervals 1 and 2.

There are notable changes in the trunk channel geometries within individual lobe complexes (for example Figures 7, 8, 10-13). Our observations suggest that the changes in sediment distribution patterns, between successive intervals through each lobe complex, are driven both by the underlying structure and by lobe compensation. There are several intervals where it is possible to see lateral movement of a lobe or the avulsion of a trunk channel system associated with relict high topography from an earlier lobe. A detailed example can be seen in Figure 15 where the amplitude extractions show that a small lobe has laterally migrated eastwards. The scale of these lateral migrations and corresponding compensational stacking of individual lobes is similar to that observed in outcrop data in the Karoo Basin, South Africa by Prélat et al. (2009), as they illustrate in their correlation panel of thinning and stacking of individual lobe systems (Figure 15 C)

COMPARISON TO OTHER SYSTEMS

To use these lobe complexes as analogues for other buried ponded successions that may not be as well-imaged, we compare our results to ponded lobe complexes elsewhere. We use a variety of, subsurface seismic, modern seafloor and outcrop studies for this comparison.

Seismic Studies

Studies of lobe complexes have mostly been carried out in the shallow seafloor where the distribution of lobe complexes has been extensively mapped and some vertical architecture resolved (for example Beaubouef et al., 2003, Booth et al., 2003, Adeogba, 2005, Saller, 2008, Hay, 2012, Prather et al., 2012) However, the limits of the resolution mean that these systems have only been imaged to the lobe scale and the individual channels within these lobes are difficult to distinguish in the amplitude extraction maps.

The lobes observed in this minibasin are similar in size and scale to those described from salt and shale-influenced basins elsewhere. However, documented examples typically consist of a series of MTCs overlain by distributary channel-lobe complexes (Prather et al., 1998, Beaubouef and Friedmann, 2000, Adeogba, 2005). MTCs and lobe complexes are observed within our study area, but not necessarily together in the systematic repeated sequence described by other authors. Different degrees of ponding are also observed in other deep-water settings: ponding within almost completely enclosed basins such as occurs in the Gulf of Mexico (e.g. Booth et al. 2003) or less strongly ponded, stepped shelf systems where ponding occurs briefly before the gradient of the system flattens out and bypass occurs (e.g. Adeogba et al., 2005, Hay et al., 2012). The ponding observed in our example is somewhere between these extremes with an almost completely enclosed minibasin, but containing less repeated cycles than those in the Gulf of Mexico. A discussion of the key features of these different types of systems is worthwhile as it allows characteristics common to all settings to be identified.

Booth et al. (2003) investigate the development of confined lobe complexes in the Auger and Macaroni Fields, Gulf of Mexico. They see differences in the stratigraphic architecture that they attribute to palaeo-bathymetric controls on the basin. The Auger Basin is smaller than the minibasin studied here but is also confined by salt structures on each flank. The Auger basin has a width of approximately 2.5 km (1.6 mi) and length of 10 km (6.2 mi) compared to the ca. 15 km (9.3 mi) length and 10 km (6.2 mi) wide basin of our study. A series of sandy lobe complexes onlap the salt structures and are often capped by erosional channel complexes or MTCs. The lobe complexes are very similar in style to those observed in the study area in Angola. The Auger Field also has a normal fault that was active during the deposition of the lobe complexes. Booth et al. (2003) state that there was considerable expansion in sediment thickness on the down-thrown side of the fault and that the expanded section has a higher percentage of sand. They note that the channelised sections are generally less erosive on the downthrown side of the fault, with better sand preservation seen in wells. These observations are somewhat analogous to the changes seen in this dataset within the P40 – P50 unit, where amplitude extractions show that the channels are much better preserved in the hangingwall and cluster near the fault, trending parallel to the fault orientation. Due to the lack of well data it is not possible to comment on the sand content of the sediments observed on the down-thrown side of the normal fault within our study area. However, the clustering of high amplitude channels in the P40 – P50 interval suggest a higher sand content in this area (Figure 12).

Hay (2012) observes similar patterns in the spatial location and development of a lobe complex in the Kwansa Basin, Angola to those seen in this study of the Lower Congo Basin, Angola. She observes a confined feeder-channel network that expands on entry to the basin to form depositional lobes, and that the deposition of the lobes changes as the basin topography varies. She documents the erosional front shifting up-dip during the overall down-dip propagation of the system. A similar pattern to this is visible within the P20 – P30 sequence in this study where the lobes appear to move progressively further into the basin whilst the entry point widens (Figures 7A-D), suggesting increased erosion.

MODERN SEAFLOOR STUDIES

Studies of deep-water lobe complexes on the modern seafloor use high resolution sidescan sonar, back scatter and bathymetric data to explore these systems in many locations around the world including the Gulf of Mexico, Corsica, Barbados, Angola and Indonesia (Belderson et al., 1984, Twichell et al., 1992, Ercilla et al., 1998, Kenyon et al., 2002, Deptuck et al., 2008, Jegou 2008, Prélat et al. 2010, Pichot et al. 2016). High-resolution acoustic imaging is often coupled with information from piston cores to aid understanding of the lithology. However, imaging in this way only allows a snap-shot in the development of a lobe complex to be observed as very few details of the vertical architecture are resolvable. This makes it difficult to understand the evolutionary history of the system.

The scale of the lobe complexes and the patterns observed as they develop within the Angolan minibasin are very similar to those recorded by Twichell et al. (1992) on the modern-day outer Mississippi Fan in the deep-water Gulf of Mexico although the lobes have formed in different settings (base of slope as opposed to intra-slope basin) and at a very different scale. The Twichell et al. study observed crosscutting channels within the lobe complex using sidescan sonar data and they infer that these relationships indicate that only one channel was active at a time. Hence many depositional events were responsible for the construction of each lobe. Cross-cutting relationships are frequently observed in the amplitude extractions shown in our work and therefore we can infer many individual depositional events also formed the lobe complexes studied here (for example see Figures 8 and 13). The channels observed towards the distal end of the fan by Twichell et al. (1992) are on the same scale as the smallest channels seen within the lobes in the study area. In general those recorded by the backscatter data over the Mississippi Fan are typically less than 100 m (328ft) wide and have a relief of less than 2 m (6.6 ft), whilst those detailed in our study are on average 90 m (295 ft) wide (Figure 9). The termination patterns of the lobes in our study are quite similar to the 'fronds' observed by Twichell et al. (1992). Piston cores on the Mississippi Fan lobes been used to re-interpreted the fronds as the deposits of thin muddy debrites (Talling et al. 2010).

OUTCROP STUDIES

Outcrop studies exploring deep-water lobe complexes are extensive with work carried out throughout the world including the Karoo Basin in South Africa, the Pennsylvanian Ross Formation in County Clare, Ireland, the Permian Brushy Canyon Formation in West Texas, the Precambrian Kongsfjord Formation, Norway and the upper Miocene Laga Basin in the Central Apennines, Italy (Carr and Gardner, 2000, Gardner and Borer, 2000, Sullivan et al., 2000, Drinkwater and Pickering, 2001, Gardner et al. 2003, Wach et al., 2003, Sullivan et al., 2004, Hodgson et al. , 2006, Hodgson, 2009, Prélat et al., 2009; van der Merwe et al. 2014; Marini, et al. 2015, 2016, Spychala 2015, Hodgson et al 2016). We mostly make comparisons with the Karoo Basin and the Ross Formation outcrops as these are two of the best-studied examples in modern literature. Field work in these classic locations has allowed extensive and detailed descriptions of the facies within lobe complexes to be fully explored from proximal to distal locations and has provided insights into the vertical architecture of these systems. Due to the nature of the outcrop locations only limited scale spatial mapping of the lobe complexes has been possible, but despite this, there are several comparisons which can be drawn between the work carried out on outcrops and our high-resolution seismic study.

Previous studies using outcrop data have sub-divided the lobe complexes into proximal, medial and distal fan settings according to key characteristics like channel size, aspect ratio of the sand bodies (width to thickness ratio), and key reservoir characteristics such as net-to-gross and the continuity of sand bodies (Sullivan et al., 2000). In the lobe complexes imaged within the P20 – P30 and younger units the proximal fan is dominated by feeder channels entering the basin. These are best imaged in the P20 – P30 and P40 – P50 units where they are between 250 m and 300 m wide and tend to have a high amplitude signature indicating a high sand content. As such, they are like those observed in the Ross Formation in the Clare Basin, Ireland (Figure 16A) where sand-rich amalgamated channels have been observed in outcrop (Sullivan et al., 2000, Sullivan et al., 2004).

In the Ross Formation Sullivan et al. (2004) have described a transitional domain towards the centre of the lobe complexes containing channelised and amalgamated sheet facies (Figure 16B). They are able to trace the beds as they thin and become less amalgamated from the axis to the margins of the lobes. In the Angolan study area, this domain exists towards the middle of the lobe complexes where trunk channels branch before the development of lobes: channels are more amalgamated towards the centre and thin towards their margins (Figure 14bii). The channels in the Angolan data have very similar widths to those observed in outcrop (Figure 16; Sullivan et al., 2004).

Similarities between the level of detail observed in outcrop and within this study are also apparent in the densely, channelised lobes which form in a distal location within the lobe complexes. In outcrop these have often been described as channelised sheet facies with channel amalgamation occurring within the lobe axis. Within our seismic study, high amplitude, discrete, but amalgamated, channels are frequently observed towards the centre of the lobes with lateral migration and compensational stacking implying that they thicken towards the lobe axis (Figures 8, 11, 13). This corresponds to observations made from outcrop studies in the Karoo Basin where the beds that form the individual lobes amalgamate, thicken and become sandier towards the lobe axis (Figure 17A; Prélat et al., 2009).

High amplitude fringes are imaged towards the edge of both individual lobes and the lobe complexes (Figures 15 A,B). These correspond to the location of amalgamated and layered sheets observed within the Ross Formation of the Clare Basin, Ireland (Figure 17C). In outcrop these amalgamated sheets contain a higher proportion of sand and, as such, correspond well to the amplitude signature observed in the study area. Recent studies of lobe complexes have concentrated on the idea of hybrid event beds (e.g. Haughton et al. 2003, Hodgson, 2009, Talling, 2013) located towards the fringes of lobe complexes and thought to be generated during fan initiation and growth (Hodgson, 2009). The RMS amplitude extractions reveal areas around the individual lobes at the edge of the lobe complexes with higher amplitudes compared to the surrounding area, suggesting a slightly higher sand content (Figures 15). We propose that the high amplitude fringes associated with the edges of the lobe deposits seen in Figure 15 might be the amplitude signature of such event beds sequences.

DISCUSSION OF COMPARISON WITH OTHER SYSTEMS

Comparison of other modern and ancient lobe complexes using a range of data sets indicates some common themes across the examples regardless of their setting i.e. intra-slope basin or open basin floor. All the examples of lobe complexes demonstrate both channelized facies with non-channelized facies beyond the channels. The channelized facies comprise feeder channels, trunk channels and distributary channels as defined in the Angola example described in this paper. In the isoproportional maps generated from the Angola data set there are usually multiple trunk channels imaged in each map, sometimes with complex cross cutting relationships. Comparison with outcrop studies in particular suggest that these trunk channels can be at a similar stratigraphic level but are probably slightly different ages (Figure 14a) i.e. only one lobe was active at a time.

In the Angola data we interpret the bright featureless amplitudes as non-channelized lobe deposits but the edges of this facies is often difficult to define in detail. This is perhaps to be expected due to the lateral facies changes observed in ancient systems towards the fringe of the lobes.

Perhaps surprising in the Angola data is the scope of resolvable channels across the basin with trunk and distributary channels apparently extending across the entire intra-slope basin in some intervals. A key variability in lobe complexes may be the amount of channelized and non-channelized facies which is generated. We can surmise that this may be related to a number of factors including sediment calibre, change of slope angle at the feeder channel mouth, degree of confinement of the basin (i.e. intra-slope vs. open basin floor) and external forcing (tectonics, sea-level) of the system.

CONCLUSIONS

- We describe an interval of ponded slope sediments deposited over approximately 2.7 Ma in a salt-controlled intra-slope basin approximately 10 km (6.2 mi) by 15 km (9.3 mi) in size. The ponded interval consisting of four discrete stratigraphic sequences, each of which contains one lobe complex. The shape and orientation of the lobe complexes change systematically through time. The two older lobe sequences are fed from the northeast of the basin whereas the youngest units are fed from the southeast.
- Detailed amplitude extraction maps generated from high-resolution three-dimensional seismic data allow the facies that form a lobe complex to be imaged in the subsurface in exceptional detail. The lobe complexes are composed of a feeder channel, trunk channels and lobes comprised of a diverging network of smaller distributary channels with a high amplitude rim.
- The images have been used to demonstrate that lobes and the channels within the lobe complexes respond to both bathymetry internal to the basin, through compensational stacking and lateral migration, and changes external to the basin causing the progradation and retreat of lobe complexes and the feeder channel to switch from north east to south east. We infer that the shift of the feeder channel entry point is mostly likely due to salt tectonics immediately to the east of the minibasin salt structures.
- The unprecedented level of detail at which the lobe geometries and facies have been imaged allows the facies-based observations within these sequences to bridge the gap between current research using conventional seismic data and the detail observed within outcrop studies. Comparisons can readily be made between the seismic observations and the facies observed in major outcrop study areas of lobe complexes.
- The Angola example described here builds on exisiting reservoir description frameworks for lobe complexes by providing some important analogue information

through the well-imaged planform data. This new example can be used as a unique analogue to enhance the understanding of reservoir heterogeneities within deep-water fan systems in ponded basins throughout the world.

REFERENCES

Adeogba, A. A., 2005, Transient fan architecture and depositional controls from near-surface 3-D seismic data, Niger Delta continental slope: AAPG Bulletin, v.89, p. 627-643.

Al Ja'aidi, O. S., McCaffrey, W. D. and Kneller, B. C., 2004, Factors influencing the deposit geometry of experimental turbidity currents: implications for sand-body architecture in confined basins: Geological Society, London, Special Publications, v.222, p. 45-58.

Beaubouef, R., Abreu, V. and Van Wagoner, J., 2003, Basin 4 of the Brazos–Trinity slope system, western Gulf of Mexico: the terminal portion of a late Pleistocene lowstand systems tract *in*, Shelf margin deltas and linked down slope petroleum systems: Global significance and future exploration potential: Proceedings of the 23rd Annual Research Conference, Gulf Coast Section SEPM Foundation, 2003. SEPM, p. 45-66.

Beaubouef, R. T., and Friedmann, S. J., 2000, Basin 4 of the Brazos–Trinity slope system, western Gulf of Mexico: the terminal portion of a late Pleistocene lowstand systems tract, shelf margin deltas and linked down slope petroleum systems, *in,* Roberts, H.H., Rosen, N.C., Fillon, R.H. and Anderson, J.B., eds., Shelf Margin Deltas and Linked Down Slope Petroleum Systems: Global Significance and Future Exploration Potential: GCSSEPM 23rd Annual Research Conference, p. 45-66.

Belderson, R., Kenyon, N., Stride, A. and Pelton, C., 1984, A 'braided'distributary system on the Orinoco deep-sea fan: Marine Geology, v.56, p. 195-206.

Booth, J. R., Dean, M. C., Duvernay III, A. E. and Styzen, M. J., 2003, Paleo-bathymetric controls on the stratigraphic architecture and reservoir development of confined fans in the Auger Basin: central Gulf of Mexico slope: Marine and Petroleum Geology, v.20, p. 563-586.

Brunt, R.L., Mcaffrey, W.D., And Kneller, B.C., 2004, Experimental modeling of the spatial distribution of grain size developed in a fill-and-spill minibasin setting: Journal of Sedimentary Research, v. 74, p. 438-446.

Carr, M., and Gardner, M., 2000, Portrait of a basin-floor fan for sandy deep-water systems, Permian Lower Brushy Canyon Formation, West Texas, *in* Bouma, A.H. and Stone, C.G., eds. Fine-grained turbidite systems: AAPG Memoir, v. 72 and SEPM Special Publication, v. 68, p. 215-232.

Covault, J.A., and Romans, B.W., 2009, Growth patterns of deep-sea fans revisited: Turbidite-system morphology in confined basins, examples from the California Borderland: Marine Geology, v. 265, p. 51-66.

Damuth, J.E. and Olsen, H.C., 2016, Latest Quaternary sedimentation in the northern Gulf of Mexico Intraslope Basin Province: 1. Sediment facies and depositional processes: Geosphere v. 11, p. 1689-1718.

Deptuck, M. E., Piper, D. J. W., Savoye, B. and Gervais, A., 2008, Dimensions and architecture of late Pleistocene submarine lobes off the northern margin of East Corsica: East Corsica submarine lobes: Sedimentology, v.55, 869-898.

Drinkwater, N., and Pickering, K., 2001, Architectural elements in a high-continuity sand-prone turbidite system, late Precambrian Kongsfjord Formation, northern Norway: Application to hydrocarbon reservoir characterization: AAPG Bulletin, v. 85, p. 1731-1757.

Ercilla, G., Alonso, B., Baraza, J., Casas, D., Chiocci, F. L., Estrada, F., Farrán, M., Gonthier, E., Pérez-Belzuz, F., Pirmez, C., Reeder, M., Torres, J. and Urgeles, R., 1998, New high-resolution acoustic data from the `braided system' of the Orinoco deep-sea fan: Marine Geology, v.146, p. 243-250.

Gamberi, F., and Rovere, M., 2011, Architecture of a modern transient slope fan (Villafranca fan, Gioia basin–Southeastern Tyrrhenian Sea): Sedimentary Geology, v. 236, p. 211-225.

Gardner, M.H., and Borer, J.M., 2000, Submarine channel architecture along a slope to basin profile, Brushy Canyon Formation, west Texas. *in* Bouma, A.H., and Stone, C.G., eds., Fine-grained turbidite systems: AAPG Memoir 72 and SEPM Special Publication, v. 68, p. 195–214

Gervais, A., Savoye, B., Mulder, T. and Gonthier, E., 2006, Sandy modern turbidite lobes: A new insight from high resolution seismic data: Marine and Petroleum Geology,v. 23, p. 485-502.

Haughton, P. D. W., Barker, S. P. and McCaffrey, W. D., 2003, 'Linked' debrites in sand-rich turbidite systems – origin and significance: Sedimentology, v.50, 4p. 59-482.

Hay, D.C., 2012, Stratigraphic evolution of a tortuous corridor from the stepped slope of Angola, *in* Application of the principles of seismic geomorphology to continental-slope and base-of-slope systems: Case Studies from Seafloor and Near-Seafloor Analogues, SEPM Special Publication, v. 99, p. 163-180.

Hodgson, D. M., Flint, S. S., Hodgetts, D., Drinkwater, N. J., Johannessen, E. P., and Luthi, S. M., 2006, Stratigraphic evolution of fine-grained submarine fan systems, Tanqua depocenter, Karoo Basin, South Africa: Journal of Sedimentary Research, v.76 p.20-40.

Hodgson, D. M., 2009, Distribution and origin of hybrid beds in sand-rich submarine fans of the Tanqua depocentre, Karoo Basin, South Africa: Marine and Petroleum Geology, v. 26, p. 1940-1956.

Hodgson D.,M., Kane, I.A., Flint S.S., Brunt R.L., and Ortiz-Karpf, A., 2016, Time-transgressive confinement on the slope and the progradation of basin-floor fans: Implications for the sequence stratigraphy of deep-water deposits: Journal of Sedimentary Research, v.86, p.73-86.

Jegou, I., 2008, Channel-mouth lobe complex of the recent Amazon fan: The missing piece: Marine Geology, v. 252, p. 62-77.

Jones, G., Mayall, M., and Lonergan, L., 2012, Contrasting depositional styles on a slope system and their control by salt tectonics - through-going channels, ponded fans and mass transport complexes. *in* 32nd Annual GCSSEPM Foundation Bob F. Perkins Research Conference "New Understanding of the Petroleum Systems of Continental Margins of the World"' Conference proceedings, p.503-533 (DVD).

Kenyon, N. H., Klaucke, I., Millington, J. and Ivanov, M. K., 2002, Sandy submarine canyon-mouth lobes on the western margin of Corsica and Sardinia, Mediterranean Sea: Marine Geology, v.184, p. 69-84.

Marini, M, Milli, S., Ravnås, R., Moscatelli, M., 2015, A comparative study of confined vs. semi-confined turbidite lobes from the Lower Messinian Laga Basin (Central Apennines, Italy): Implications for assessment of reservoir architecture: Marine and Petroleum Geology, v.63 p. 142-165

Marini, M., Patacci, M., Felletti, F., and McCaffrey, W.D., 2016, Fill to spill stratigraphic evolution of a confined turbidite minibasin succesion, and it's likely well bore expression: The Castagnola Fm, NW Italy: Marine and Petroleum Geology v.69, p 94-111.

Mutti, E., and Normark, W.R., 1991, An integrated approach to the study of turbidite systems, *in* Weimer, P., and Link, M.H., eds., Seismic facies and sedimentary processes of submarine fans and turbidite systems: New York, Springer-Verlag, p. 75-106.

Nelson, C. H., 1992, Upper Pleistocene turbidite sand beds and chaotic silt beds in the channelized, distal, outer-fan lobes of the Mississippi fan: Geology, v.20, p. 693-696.

Normark, W. R. 1970., Growth patterns of deep-sea fans: AAPG Bulletin, v.54, p. 2170-2195.

Oluboyo, A.P., Gawthorpe R.L., Bakke K. and Hadler-Jacobsen F., 2014, Salt tectonic controls on deep-water turbidite depositional systems: Miocene, southwestern Lower Congo Basin, offshore Angola: Basin Research v.26, p. 597–620.

Ori, G., and Friend, P., 1984, Sedimentary basins formed and carried piggyback on active thrust sheets: Geology, v. 12, p. 475-478.

Picot, M., Droz, L., Marsset, T., Dennielou, B., and Bez, M., 2016, Controls on turbidite sedimentation: insights from a quantitative approach of submarine channel and lobe architecture (late Quaternary Congo Fan): Marine and Petroleum Geology, v.72, p423-446.

Piper, D.J., Hiscott, R., and Normark, W.R., 1999, Outcrop-scale acoustic facies analysis and latest Quaternary development of Hueneme and Dume submarine fans, offshore California: Sedimentology, v.46, p. 47-78.

Posamentier, H.W., and Kolla, V., 2003, Seismic geomorphology and stratigraphy of depositional elements in deep-water settings: Journal of Sedimentary Research, v. 73, p. 367-388.

Posamentier, H.W., and Walker, R.G., 2006, Deep-water turbidites and submarine fans: SEPM Special Publication, v. 84, p. 339-520.

Prather, B. E., Booth, J. R., Steffens, G. S. and Craig, P. A., 1998, Classification, lithologic calibration, and stratigraphic succession of seismic facies of intraslope basins, deep-water Gulf of Mexico: AAPG Bulletin, v.82, p. 701-728.

Prather, B.E., Pirmez, C., Sylvester, Z., and Prather, D., 2012, Stratigraphic response to evolving geomorphology in a submarine apron perched on the Upper Niger Delta slope, *in* Prather, B.E., Deptuck, M.E., Mohrig, D., Van Hoorn, B., and Wynn, R.B., eds., Application of the Principles of Seismic Geomorphology to Continental Slope and Base-of-slope Systems: Case Studies from Seafloor and Near-seafloor Analogues, SEPM Special Publication, v. 99, p. 145-161.

Prélat, A., Hodgson, D. M. and Flint, S. S., 2009, Evolution, architecture and hierarchy of distributary deep-water deposits: a high-resolution outcrop investigation from the Permian Karoo Basin, South Africa: Sedimentology, v. 56, p. 2132-2154.

Prélat, A., Covault, J.A., Hodgson, D.M., Fildani, A., and Flint, S.S., 2010, Intrinsic controls on the range of volumes, morphologies, and dimensions of submarine lobes: Sedimentary Geology, v. 232, p. 66-76

Prélat, A., Covault J,A., **Hodgson D,M.**, Fildani, A., and Flint SS, 2010, Intrinsic controls on the range of volumes, morphologies, and dimensions of submarine lobes: Sedimentary Geology, v.232, pp.66-76.

Saller, A., 2008, Characteristics of Pleistocene deep-water fan lobes and their application to an upper Miocene reservoir model, offshore East Kalimantan, Indonesia: AAPG Bulletin, v.92, p. 919-949.

Spychala, Y.T, Hodgson D.M., Flint S.S., and Mountney, N.P., 2015, Constraining the sedimentology and stratigraphy of submarine intraslope lobe deposits using exhumed examples from the Karoo Basin, South Africa: Sedimentary Geology, v. 322, p.67-81.

Steffens, G.S., Biegert, E.K., Scott Sumner, H., and Bird, D., 2003, Quantitative bathymetric analyses of selected deep-water siliciclastic margins: receiving basin configurations for deep-water fan systems: Marine and Petroleum Geology, v. 20, p. 547-561.

Sullivan, M., Jensen, G., Goulding, F., Jennette, D., Foreman, L., and Stern, D., 2000, Architectural analysis of deep-water outcrops: Implications for exploration and development of the Diana sub-basin, western Gulf of Mexico, *in*, Weimer, P., Slatt, R. M., Coleman, J., Rosen, N. C., Nelson, H., Bouma, A. H., Styzen, M. J. & Lawrence,

D. T., eds., Deep-Water Reservoirs of the World: GCSSEPM Foundation 20th Annual Research Conference, p. 928-939

Sullivan, M.D., Foreman, J.L., Jennette, D.C., Stern, D., Jensen, G.N., and Goulding, F.J., 2004, An integrated approach to characterization and modeling deep-water reservoirs, Diana Field, Western Gulf of Mexico, an integration of outcrop and modern analogs in reservoir modelling: AAPG Memoir, v. 80, p. 215–234.

Talling, P.J., Wynn, R., Schmmidt, D.N., Rixon, R., Sumner, E., and Amy, L. 2010. How did thin submarine debris flows, carry boulder-sized clasts for remarkable distances across low gradients to the far reaches of the Mississippi Fan? Journal of Sedimentary Research, v.80, p. 829-851.

Talling, P.J., 2013, Hybrid submarine flows comprising turbidity current and cohesive debris flow: Deposits, theoretical and experimental analyses, and generalized models: Geosphere, v. 9, p. 460-488.

Twichell, D. C., Schwab, W. C., Nelson, C. H., Kenyon, N. H. and Lee, H. J., 1992, Characteristics of a sandy depositional lobe on the outer Mississippi fan from SeaMARC IA sidescan sonar images: Geology, v.20, p. 689-692.

Van der Merwe W.C., Hodgson D.M., Brunt R. L., and Flint S. S. 2014. Depositional architecture of sand-attached and sand-detached channel-lobe transition zones on an exhumed stepped slope mapped over a 2500 km^2 area. Geosphere, v. 10, p. 1076-1093.

Wach, G. D., Bouma, A. H., Lukas, T., Wickens, H. D. and Goldhammer, R. 2003. Transition from shelf margin delta to slope fan—Outcrop examples from the Tanqua Karoo, South Africa. *in* Shelf margin deltas and linked down slope petroleum systems: Global significance and future exploration potential: Gulf Coast Section SEPM 23rd Annual Research Conference, p.849-861.

Winker, C., 1996, High-resolution seismic stratigraphy of a late Pleistocene submarine fan ponded by salt-withdrawal minibasins on the Gulf of Mexico continental slope: Offshore Technology Conference Proceedings, OTC8024, p. 619-628

BIOGRAPHIES

Gemma Doughty-Jones works at BP in Africa New Ventures. She received an MSci Earth Sciences from the University of Cambridge (2008), an MSc in Petroleum Geosciences (2010) and a PhD from Imperial College London (2014). Her PhD research was on the interaction of sedimentary systems and salt tectonics. Since 2014, she has worked in BP New Ventures focussing on the Middle East and Africa.

Mike Mayall, has a B.Sc. degree from Cardiff University and an M.Sc. degree and Ph.D. in sedimentology from the University of Reading. He joined BP in 1980 and worked in many parts of the world, ending his career as a senior advisor in sedimentology. He now works as a consultant and is a visiting professor at Imperial College London.

Lidia Lonergan is a Reader in Geotectonics at Imperial College London. She has a Geology degree from Trinity College, Dublin and a D.Phil. from Oxford University. She has previously worked at Shell Research in the Netherlands and was a research fellow at BP Exploration. She was an AAPG Distinguished Lecturer (North America) in 2002/3. Her current main research focus is the interaction of deformation and sedimentation in deep-water settings.

Figure Captions

Figure 1. Location of the ponded area with respect to the main structures within the basin. This shows the maximum extent of the ponded sediments. Areas A to F refer to the main structural elements forming the basin. The high-resolution seismic data does not extend further south than the Area E label and the blue channel outlines are younger systems that cut the ponded succession. Red lines indicate the locations of seismic sections referred to in later figures.

Figure 2. Seismic line across the basin showing the salt bodies constraining the ponded basin and the two intervals of ponded sands between 9.7 and 5.6 Ma. The uppermost of these intervals, between 5.6 and 8.3 Ma, is the focus of this paper. Location of line shown in Figure 1.

Figure 3 (A) Model for a lobe complex showing the hierarchy of depositional elements (based on Prélat et al., 2010). (B) Lobe complex imaged using a root mean squared (RMS) amplitude extraction across a variable window (maximum thickness 25 m towards centre of minibasin) from sequence 4. This image is used to summarise the terminology used in this paper with a feeder channel, trunk and distributary channels, lobe complex (orange), lobes (x and y yellow), and lobe elements (red). The present day salt diapir locations are also shown in light pink along with the normal fault, active at the time of lobe complex deposition (white). (C) A root mean squared (RMS) amplitude extraction map through the interval between the green (P50) and the red horizons (detail of B). The channels are clearly imaged on the map but more cryptic on the vertical seismic lines and show as subtle convex-up features and/or brighter amplitudes.

Figure 4 (A) E-W and (B) N-S cross-sections though the ponded basin. Note two bright amplitude intervals separated by a dimmer amplitude zone. The younger of the two intervals has been analysed in detail. The surfaces (P10-P50) that define the four sequences within the younger ponded interval are shown. A younger channel cuts through the sequence in the north of the basin. The basin is bound to the east and west by folded anticlinal structures onto which the packages onlap. Line locations shown in Figure 1. **MTC = mass transport complex.**

Figure 5. Isopach maps showing the sediment thickness through the ponded interval. Note that the edges of the lobe complexes could be, in part, a result of the resolution of the data. A thinner sequence below resolution of the seismic i.e. 6-10 m (19.7-32.8 ft)may extend further in to the basin. (A) P10 – P20 unit (oldest interval) where the sediment is thickest in a triangle spreading out from the north-east and thinning towards the south, (B) P20-P30 unit which has thicker sediment either side of the previous high in the P10 – P20 unit whereas in (C) within the P30 – P40 unit the sediment is thickest in the southeast, something which continues in (D) P50 – P40 unit where the thickest sediment is again in the east of the minibasin. (E) Seismic cross-section, located on (C, D) across normal fault. Horizons ages (in Ma) on left-hand side. Note sediment growth across fault during P30-40 in particular.

Figure 6. P10-P20 RMS amplitude maps of two isoproportional intervals. (A) Oldest interval 1; (B) Younger interval. Note the location of the younger channel in the north of the minibasin that has cut through the entry point for sediments to the sequence studied. Dashed red lines indicated location of younger MTC units. Vector means for channel orientation data in the rose diagrams are given in Table 1.

Figure 7. RMS amplitude extraction maps generated using isoproportional intervals within the P20 – P30 unit. Interval 1 is the oldest and Interval 4 is the youngest within the P20 – P30 unit. Vector means for the inset channel orientation data are given in Table 1.

Figure 8. Annotated diagrams showing how the lobe complex develops within the four intervals that comprise the P20 – P30 unit. The maps clearly show the progradation of the lobe complex into the basin through all intervals and compensation stacking patterns between intervals 2 and 3 (B) and 3 to 4 (C).

Figure 9. Width measurements for the channels mapped within the isoproportional intervals in the P20-30 (A), P30-40 (B) and P40 – P50 (C) units. M = mean; SD = standard deviation; n = number of samples.

Figure 10. RMS amplitude extraction maps from the P30 – P40 unit north of the normal fault highlighting variations in the extent of the fan lobe complex through the history of the minibasin. Note that maps start at Interval 3 as Intervals 1 and 2 contain predominantly MTCs. Vector means for the channel orientation data on the rose diagrams are given in Table 1.

Figure 11. A composite summary showing how the fan complex develops during the P30 – P40 unit. Note how the system steps away from the western edge of the basin during Interval 5. Compensational stacking at the lobe scale is also clearly visible between Intervals 3 and 4.

Figure 12. A series of isoproportional amplitude extractions from the P40 – P50 interval, north and south of the normal fault. Note how the entire lobe complex in this unit has a high-amplitude fringe. The rose diagrams show orientation data for channels north of the fault. Vector means for the channel orientation data are given in Table 1.

Figure 13. A composite summary showing how the channels within the ponded fan systems vary through the history of the basin within the P40 – P50 unit. The change in channel orientation and development of an entry point south of the normal fault are clearly seen.

Figure 14. Summary of the development of lobe complexes, details in text. (A) P10-P20 input point from the northeast, lobe complex back-steps through time. (B) P20-P30 input point from the northeast, lobe complex progrades through the sequence. (C) P30-P40 input point has switched to the southeast, lobe complex back-steps through time. (D) P40-50 input point is from the southeast, lobe complex fills basin with lobe switching and some progradation to the NE.

Figure 15. (A) Un-interpreted RMS amplitude extraction map highlighting the main channel and lobe systems within P40 – P50, interval 4 alongside (B) an annotated image showing the main fan outlines and also highlighting the high amplitude fan fringes. White shows high amplitudes and black low amplitudes indicating sand and shale respectively. Red line shows location of inferred similarities at same scale as (C) which shows compensational stacking observed at the lobe scale in a schematic correlation panel from the Karoo Basin, South Africa, modified from Prélat et al. (2009).

Figure 16. (A) Proximal channels observed in the Ross Formation by Sullivan et al. (2000, 2004) (i) compared to (ii) feeder channels on a similar scale seen within the lobe complex within P40 – P50, Interval 4. (B) Compensational stacking observed within the transitional domain observed in (i) outcrop data from the Ross Formation, County Clare by Sullivan et al. (2004, used with permission of AAPG) and (ii) commonly within the transitional domain of the fan lobe complexes in the study area, as imaged here in P40 – P50 interval 4. The red line shows 1 km (0.6 mi) on the amplitude extraction map, showing a similar distance as illustrated in the sketch cross-section.

Figure 17. (A) A cross section through amalgamated and densely channelised lobes in an outcrop in the Karoo Basin (Prélat et al. 2009) compared to (B) an RMS amplitude map showing a similar area within the lobe complex in the P30 – P40, Interval 2. (C) The layered

and amalgamated sheets observed in outcrop section in the Ross formation, County Clare which we interpret as being outcrop equivalents of the high amplitude fringes observed in the study area towards the edges of individual lobes and lobe complexes (D). Cliff c.15 m (49 ft) high.

Interval name	Vector Mean ±2SD	R	n	Width (m; ft)	SD	n
P10_P20_i1	212° ± 7°	0.74	170			
P10_P20_i3	218° ± 7°	0.55	339			
P20_P30_i1	207° ± 9°	0.41	377	86 (282)	58	58
P20_P30_i2	216° ± 7°	0.53	338	116 (351)	65	39
P20_P30_i3	231° ± 5°	0.53	170	94 (308)	48	72
P20_P30_i4	247° ± 9°	0.31	377	104 (341)	46	76
P30_P40_i3	309° ± 4°	0.46	420			
P30_P40_i4	316° ± 4°	0.57	846	97 (318)	38	97
P30_P40_i5	314° ± 4°	0.60	832	96 (314)	43	51
P30_P40_i6	307° ± 5°	0.42	1229	109 (358)	49	53
P40_P50_i1	288° ± 7°	0.34	987	135 (443)	54	32
P40_P50_i2	302° ± 8°	0.34	794	100 (328)	52	25
P40_P50_i3	305° ± 7°	0.34	1033	86 (282)	41	26
P40_P50_i4	325° ± 5°	0.42	987	103 (338)	51	31

Table 1. Circular vector means, R (resultant length) value and n (number of measurements) for channel orientation data shown in Figures 6, 7, 10 and 12. R varies from 0 to 1; a value close to 1 indicates little variation in orientations. Average channel width, standard deviation and number of measurements (n) for data in Figure 9.

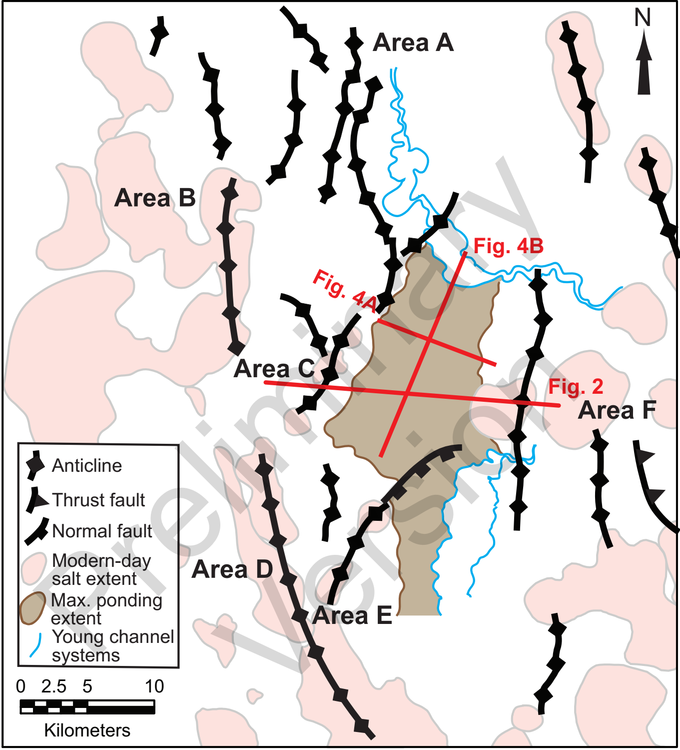

Figure 1 Doughty-Jones et al.

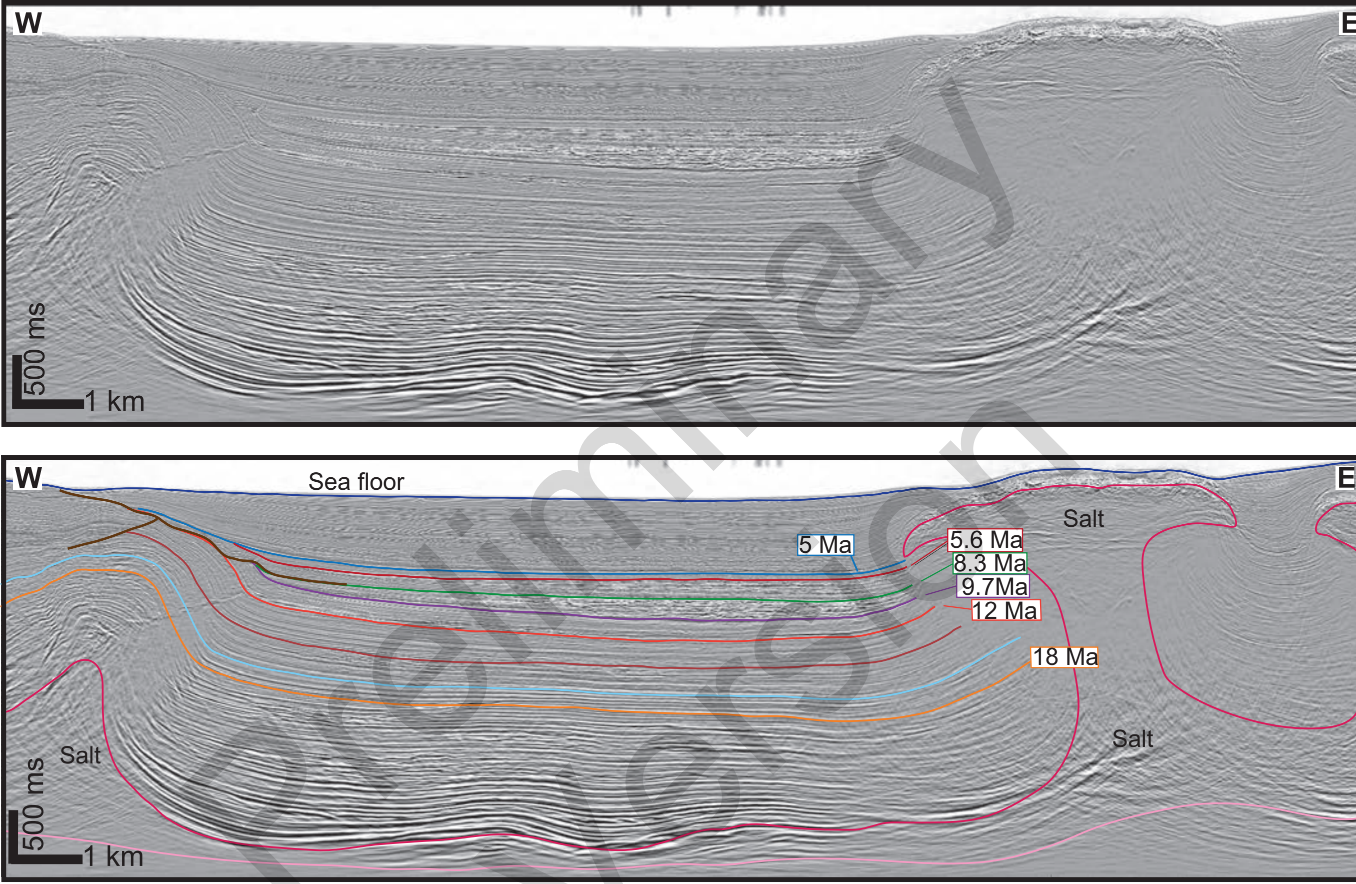

Figure 2. Doughty-Jones et al.

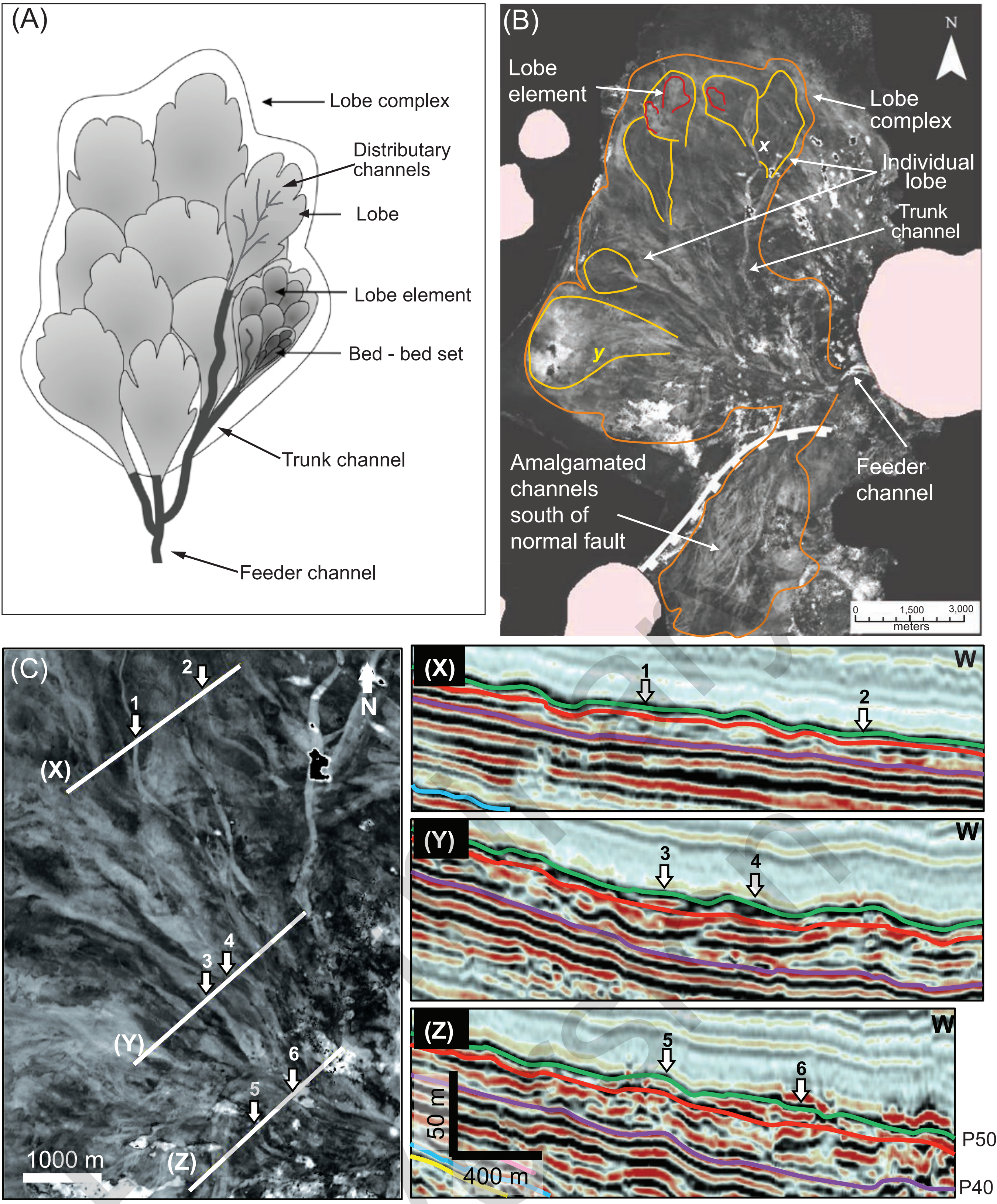

Figure 3 Doughty-Jones et al.

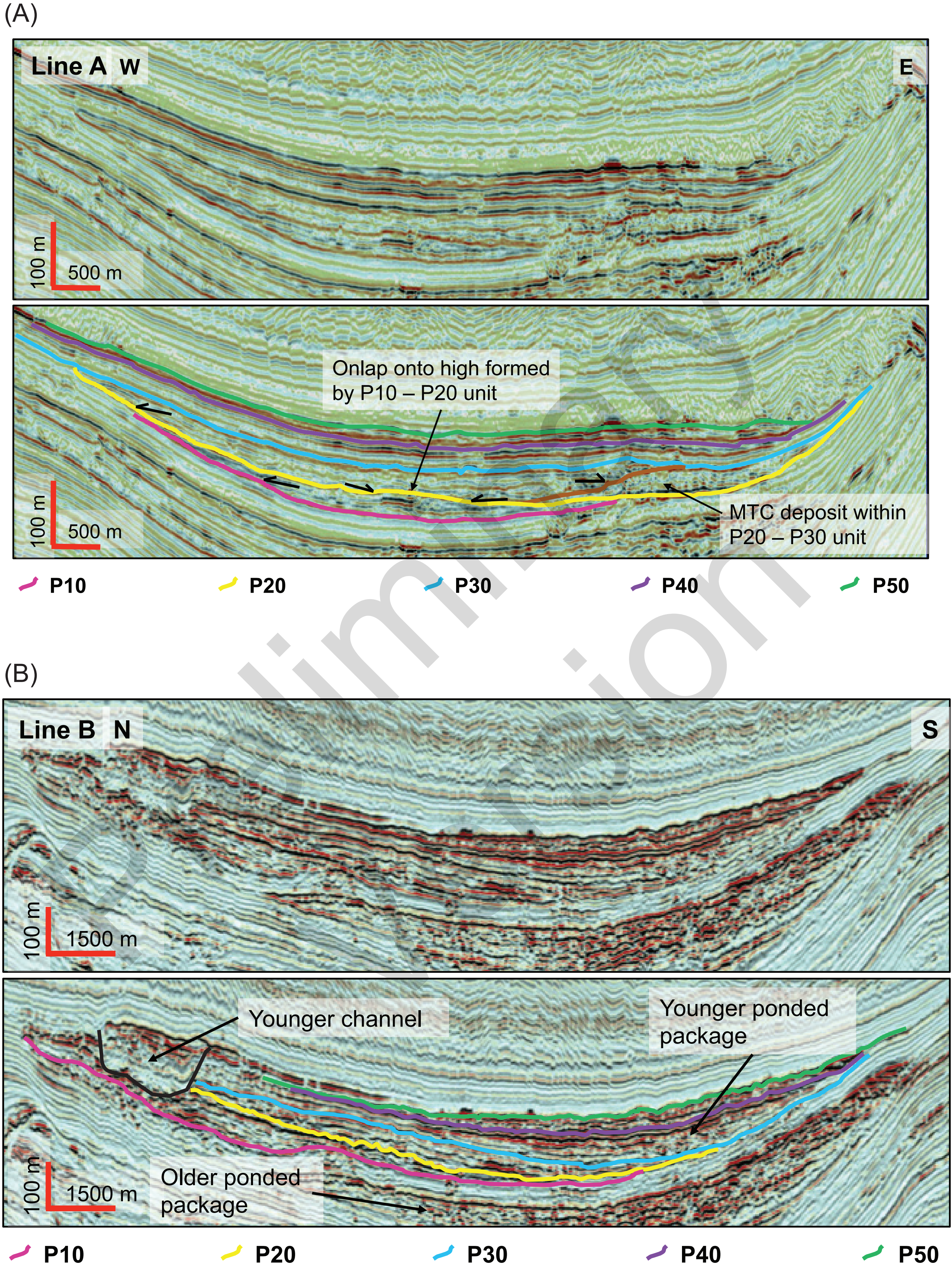

Figure 4 Doughty-Jones et al.

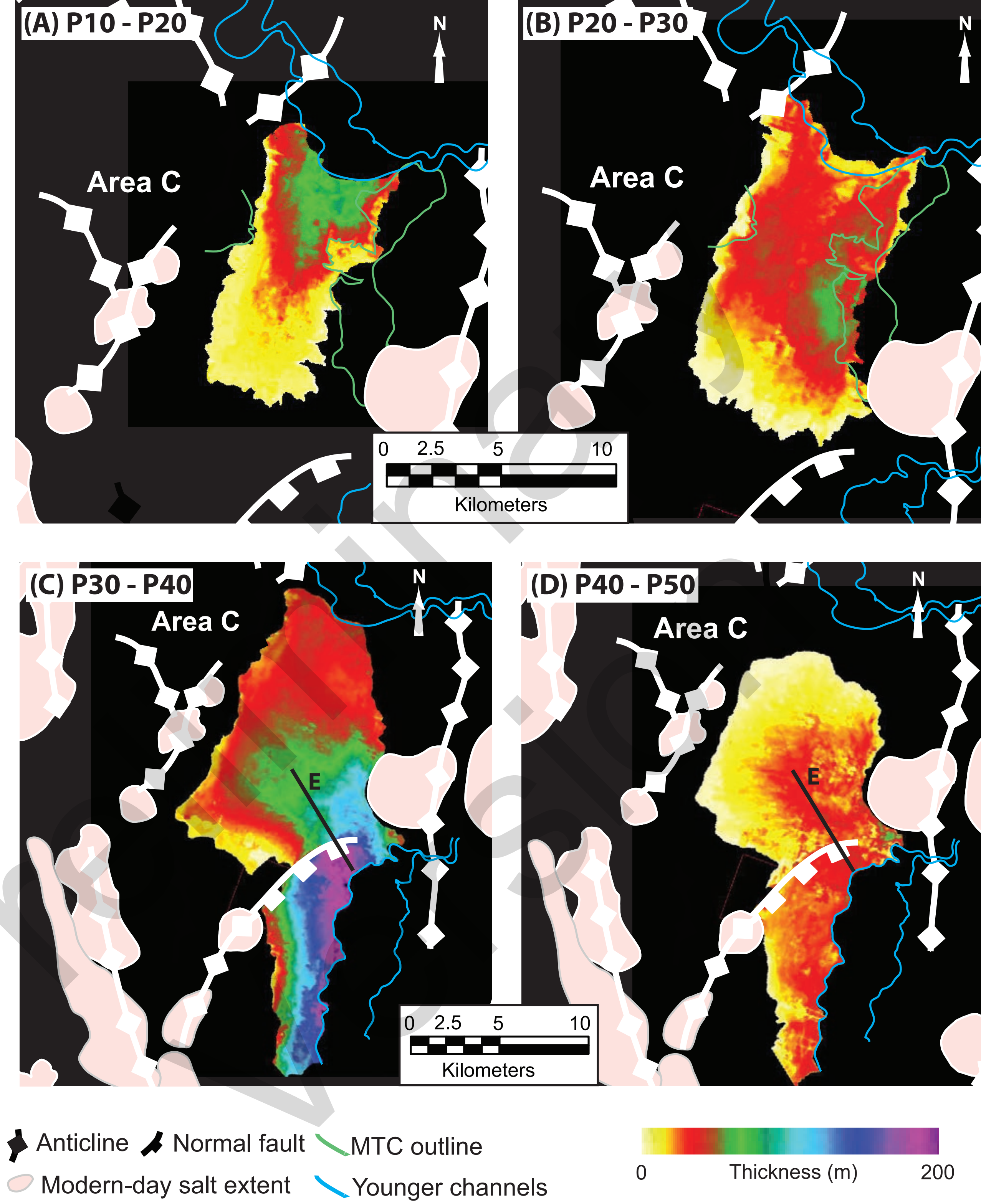

Figure 5 A-D; Doughty-Jones et al.

(E)

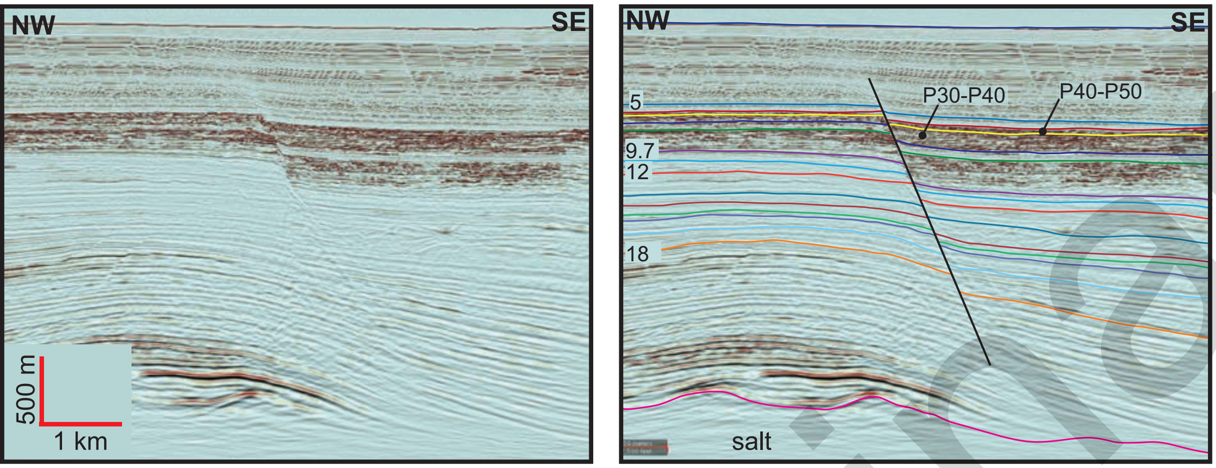

Figure 5 E Doughty-Jones et al.

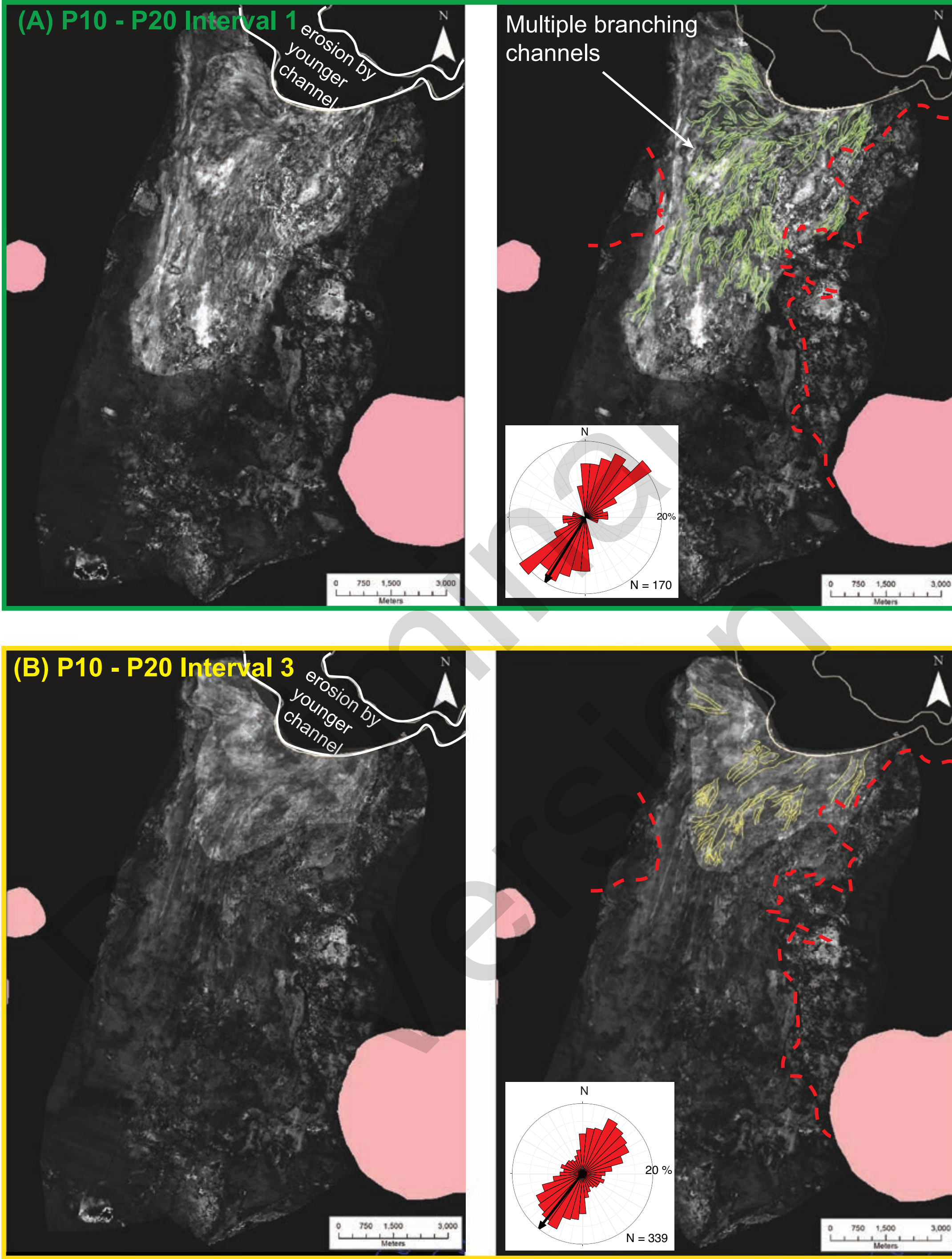

Figure 6 Doughty-Jones et al.

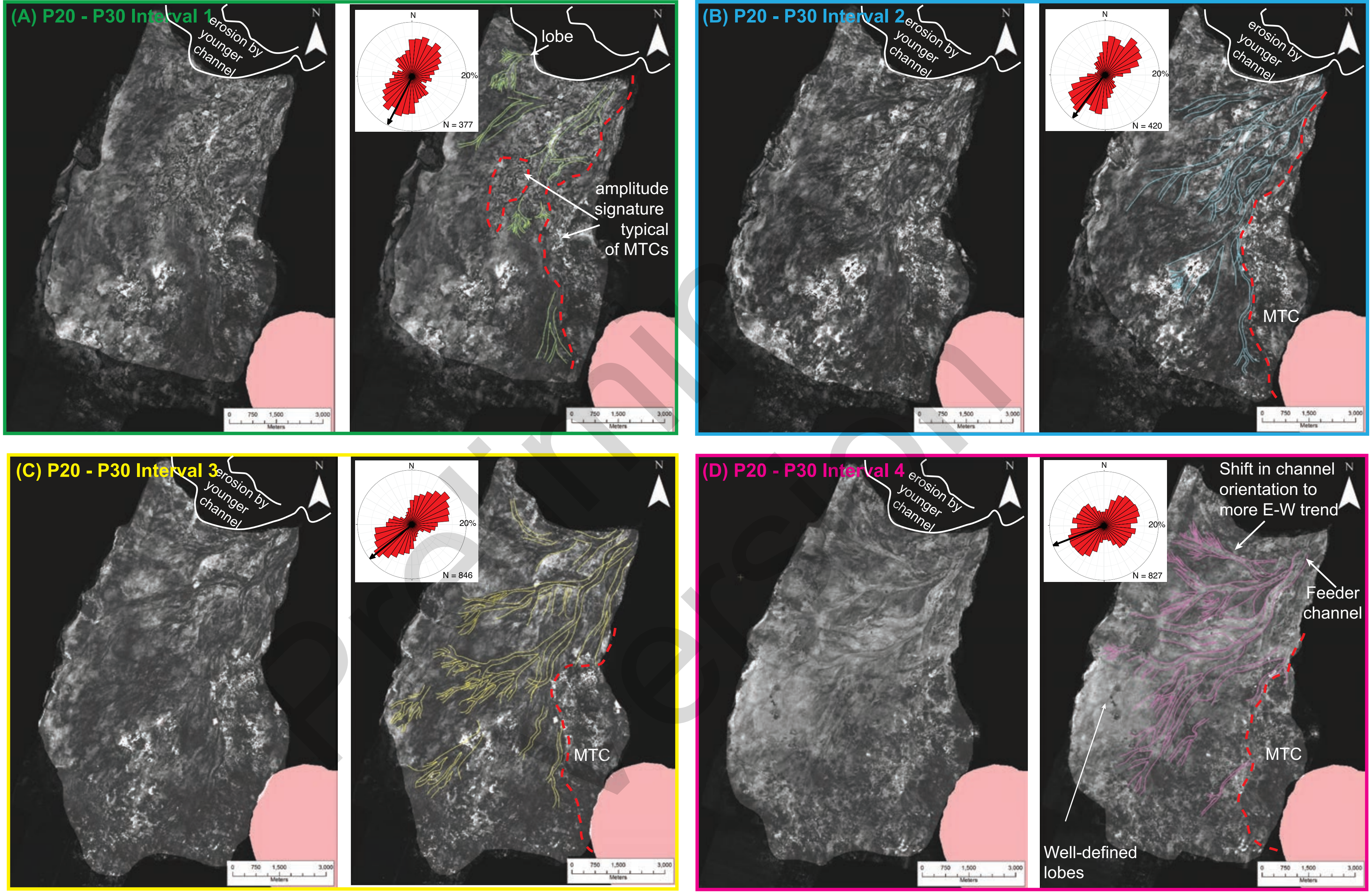

Figure 7 Doughty-Jones et al.

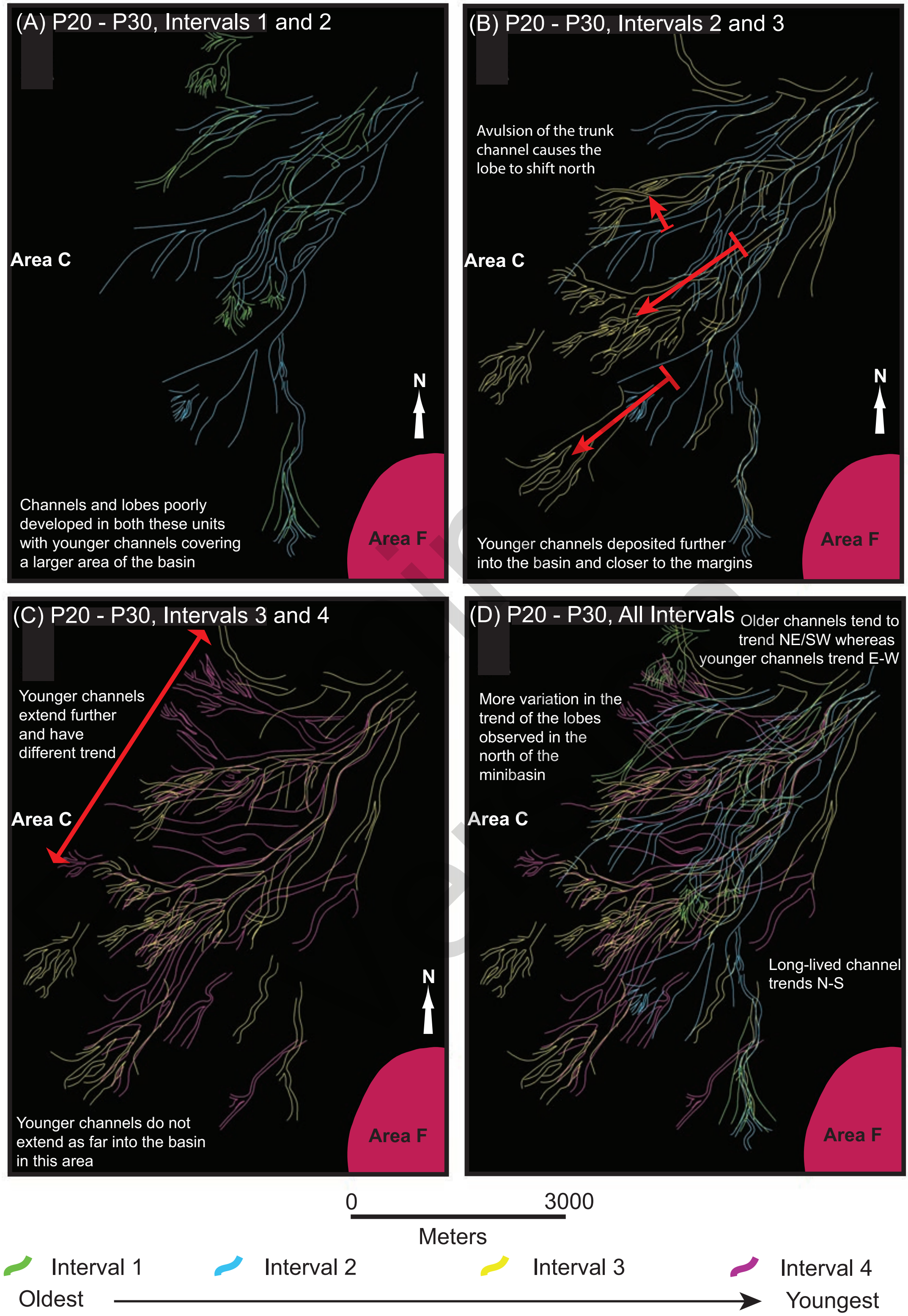

Fig 8, Doughty -Jones et al.

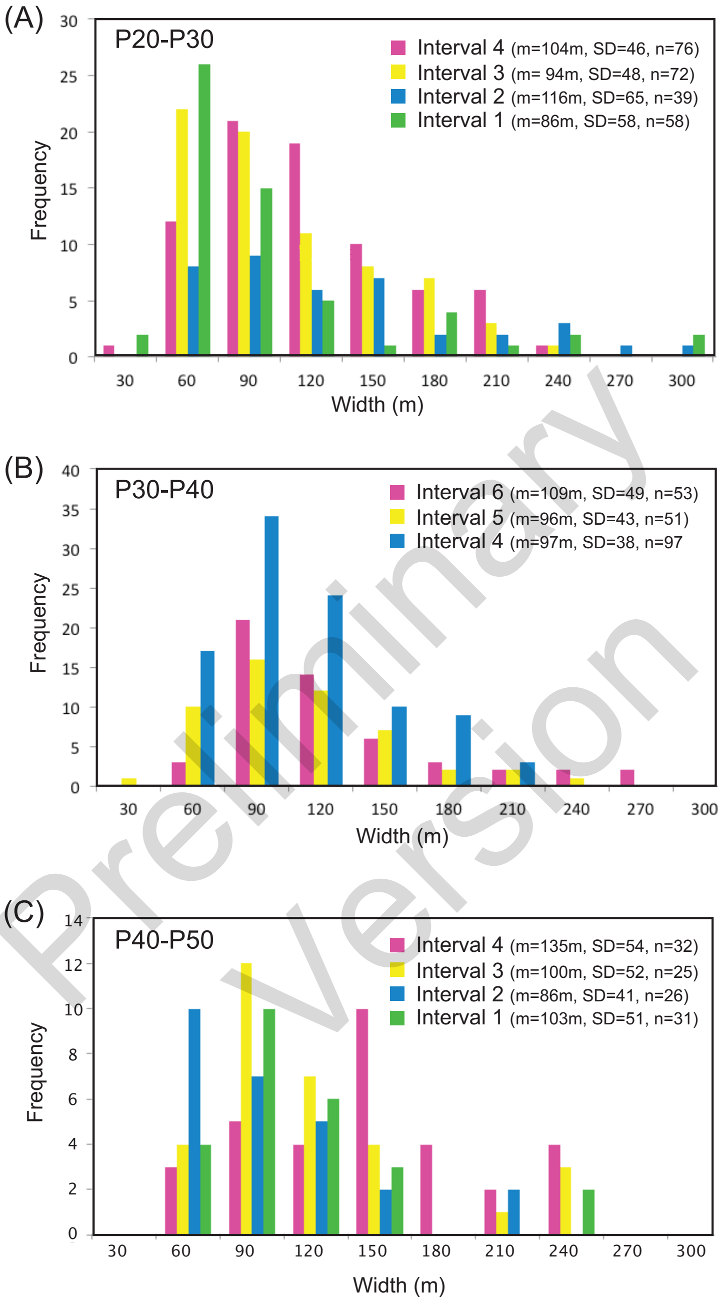

Fig 9. Doughty -Jones et al.

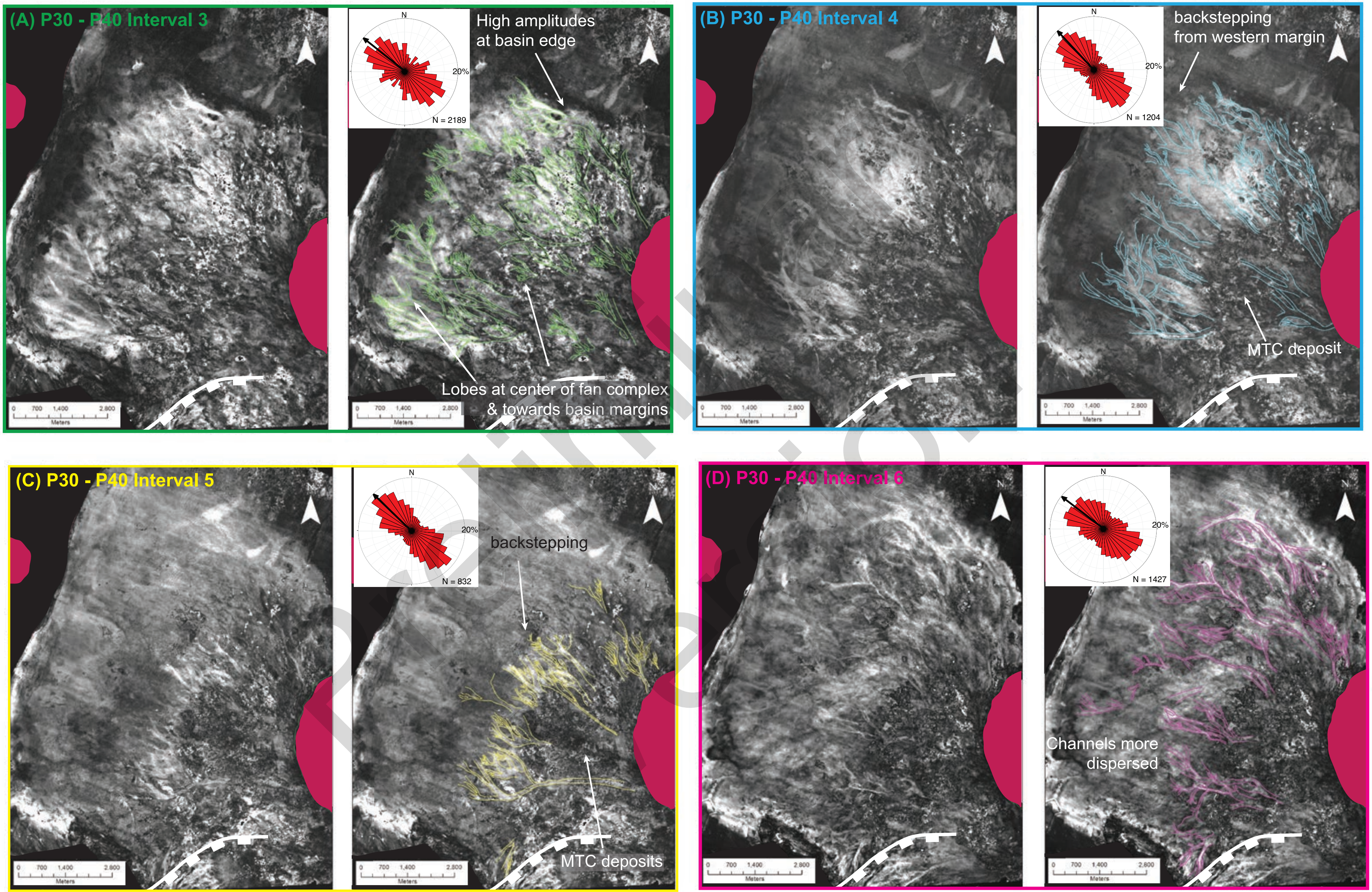

Fig 10 Doughty-Jones et al.

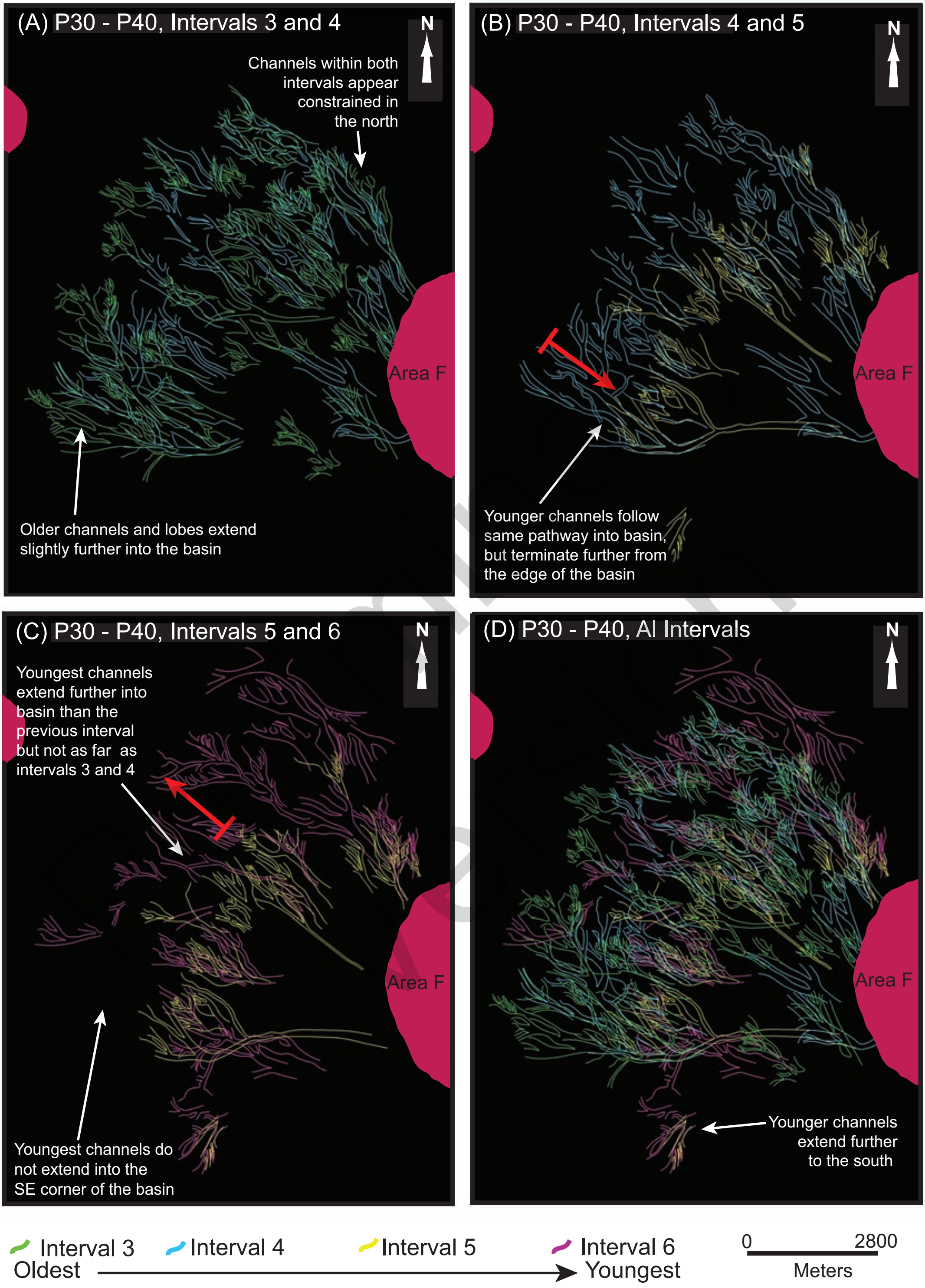

Fig 11 Doughty-Jones et al.

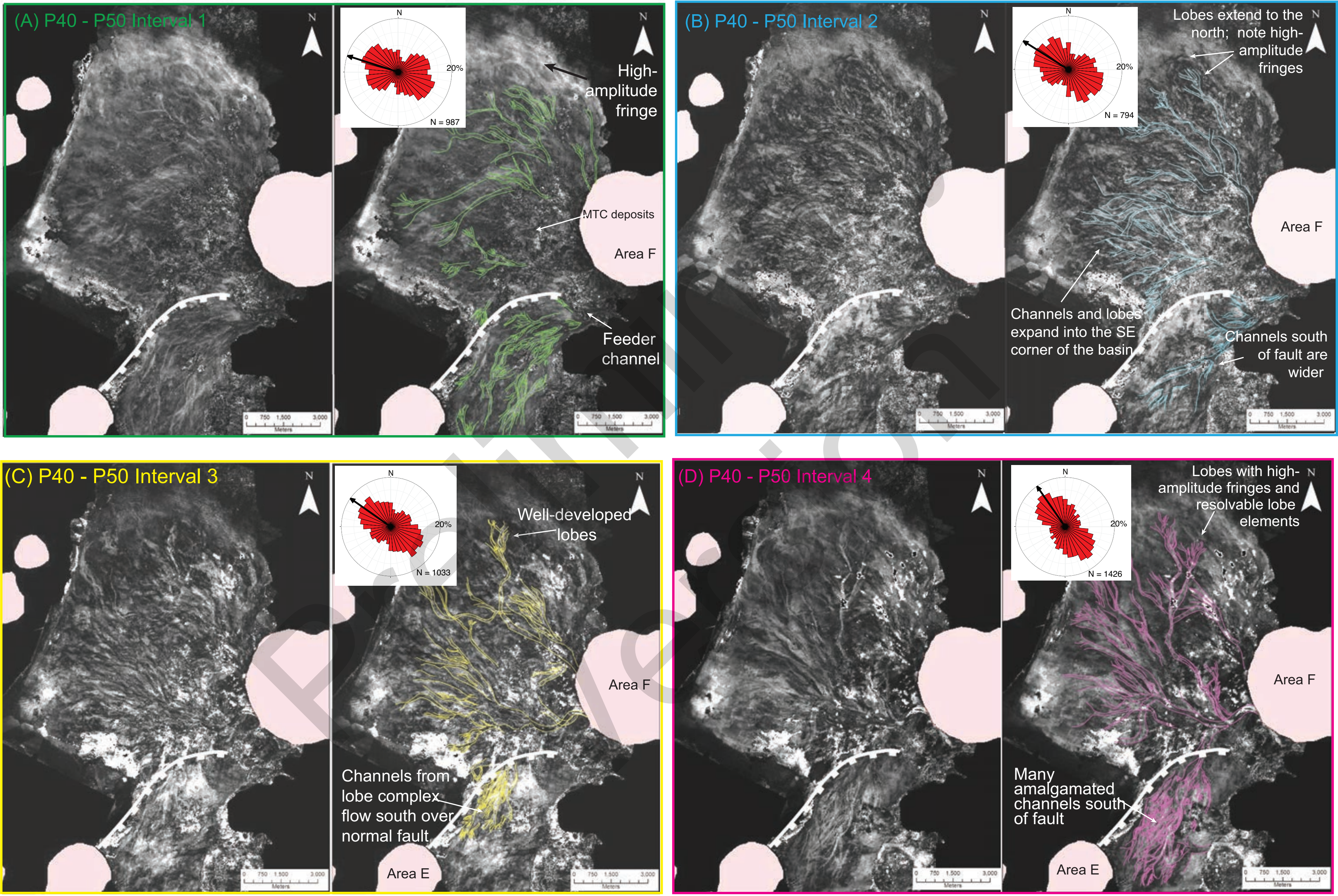

Fig 12 Doughty-Jones et al.

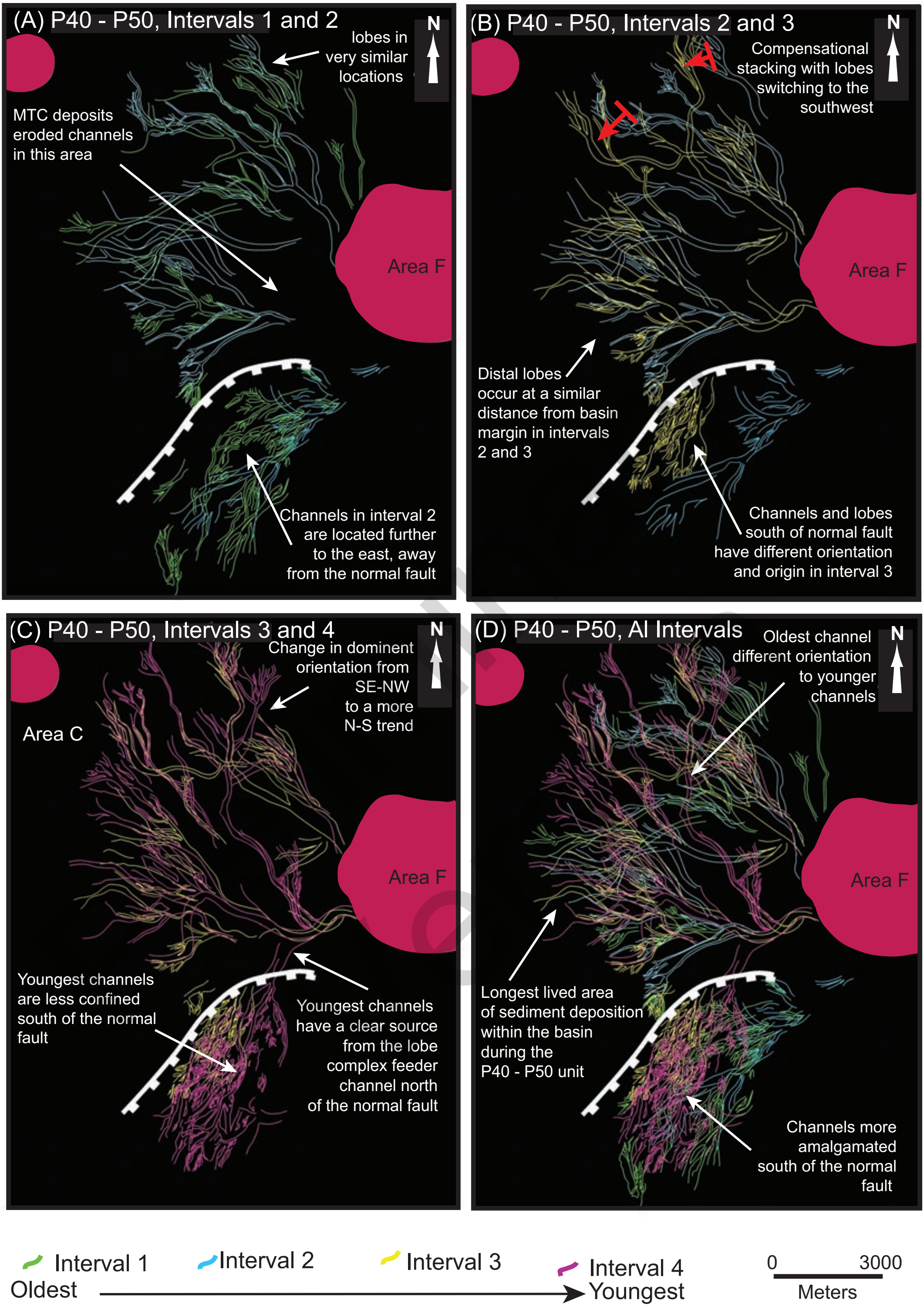

Fig 13 Doughty-Jones et al.

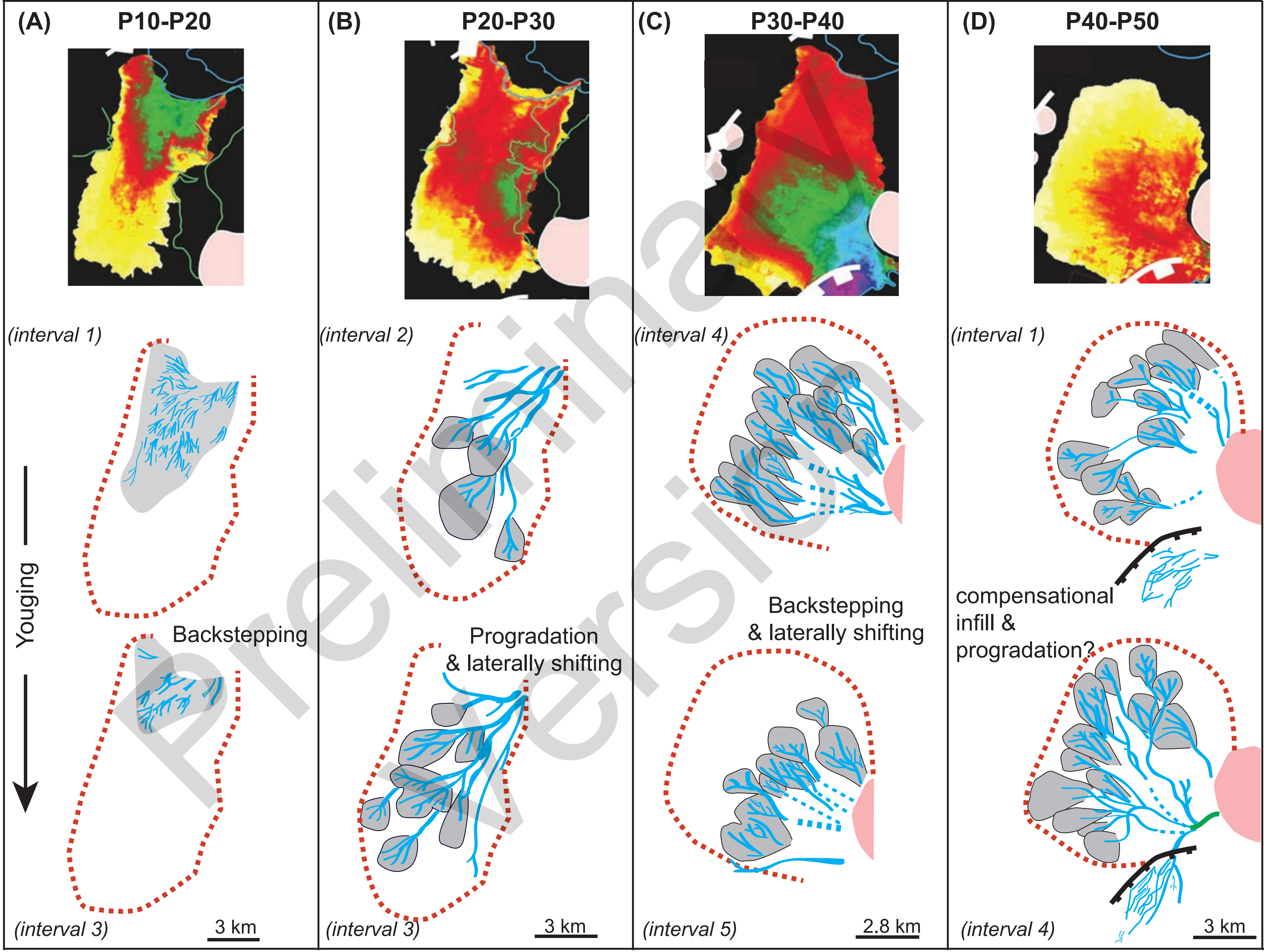

Figure 14 Doughty- Jones et al

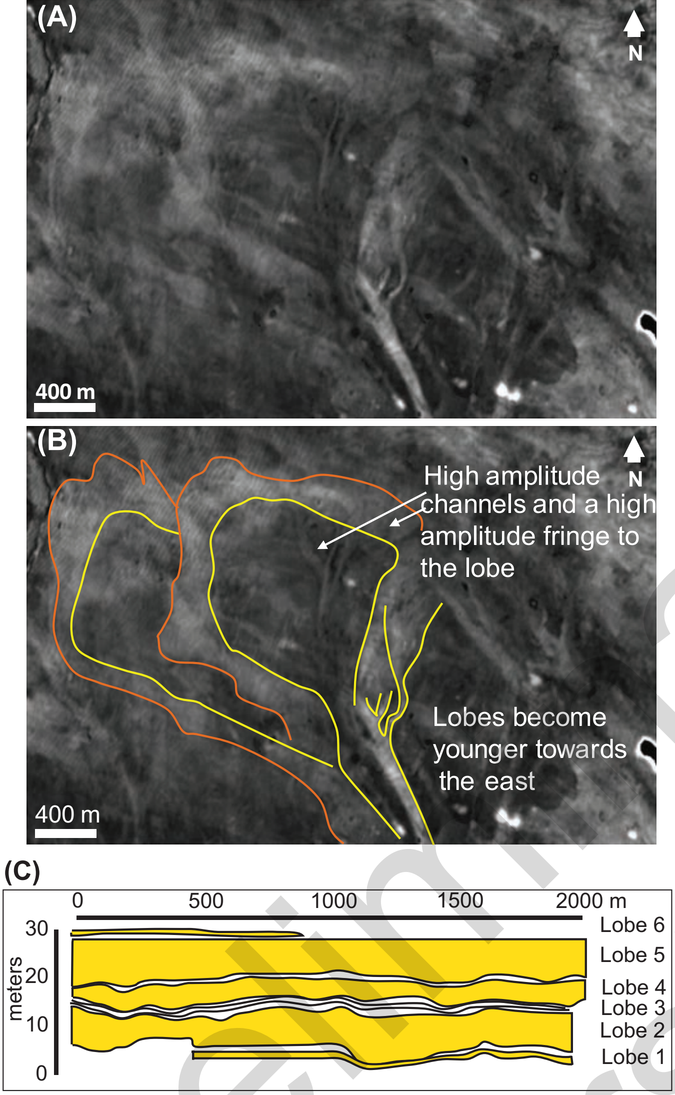

Fig 15 Doughty-Jones et al.

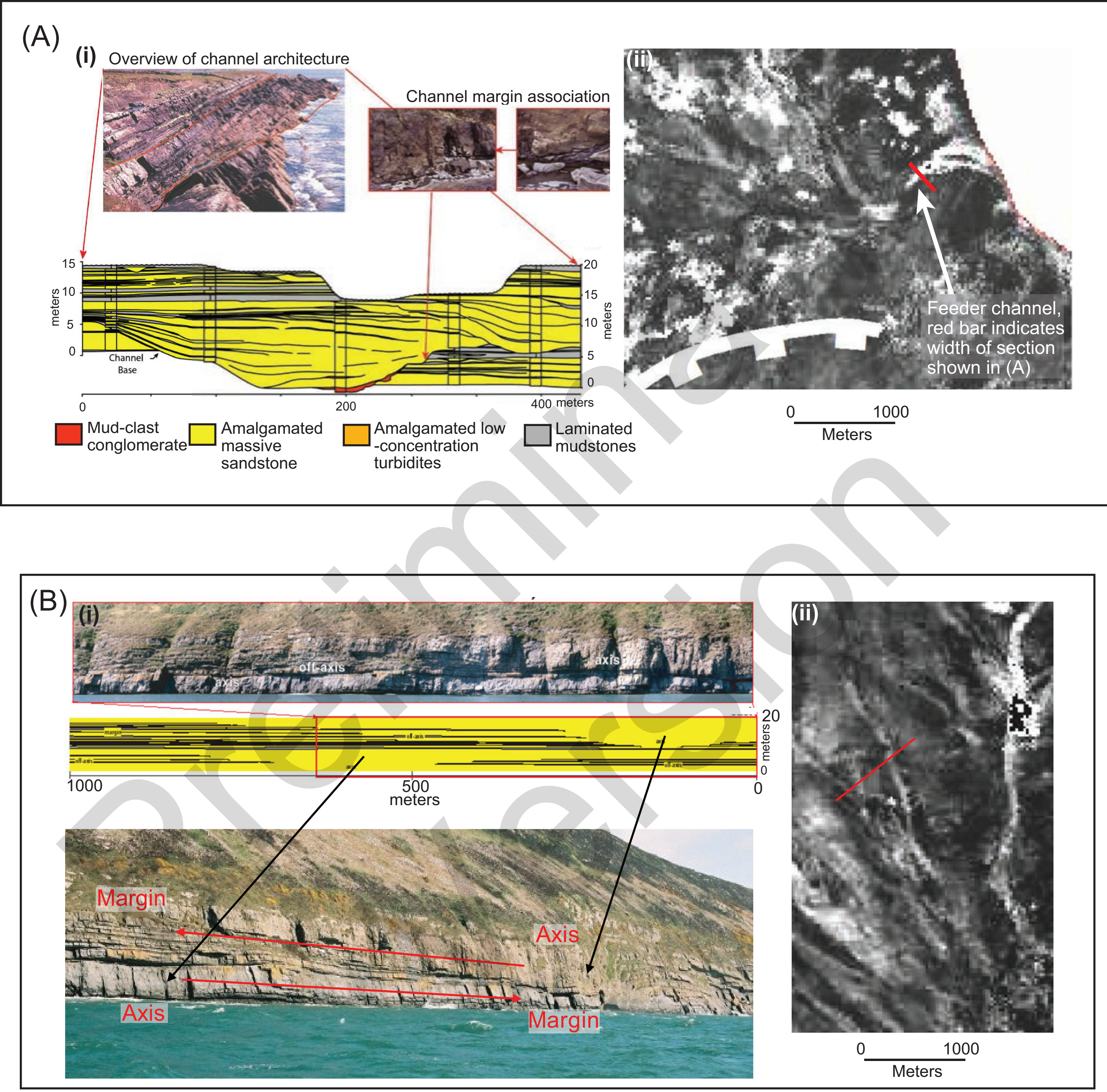

Fig 16 Doughty-Jones et al.

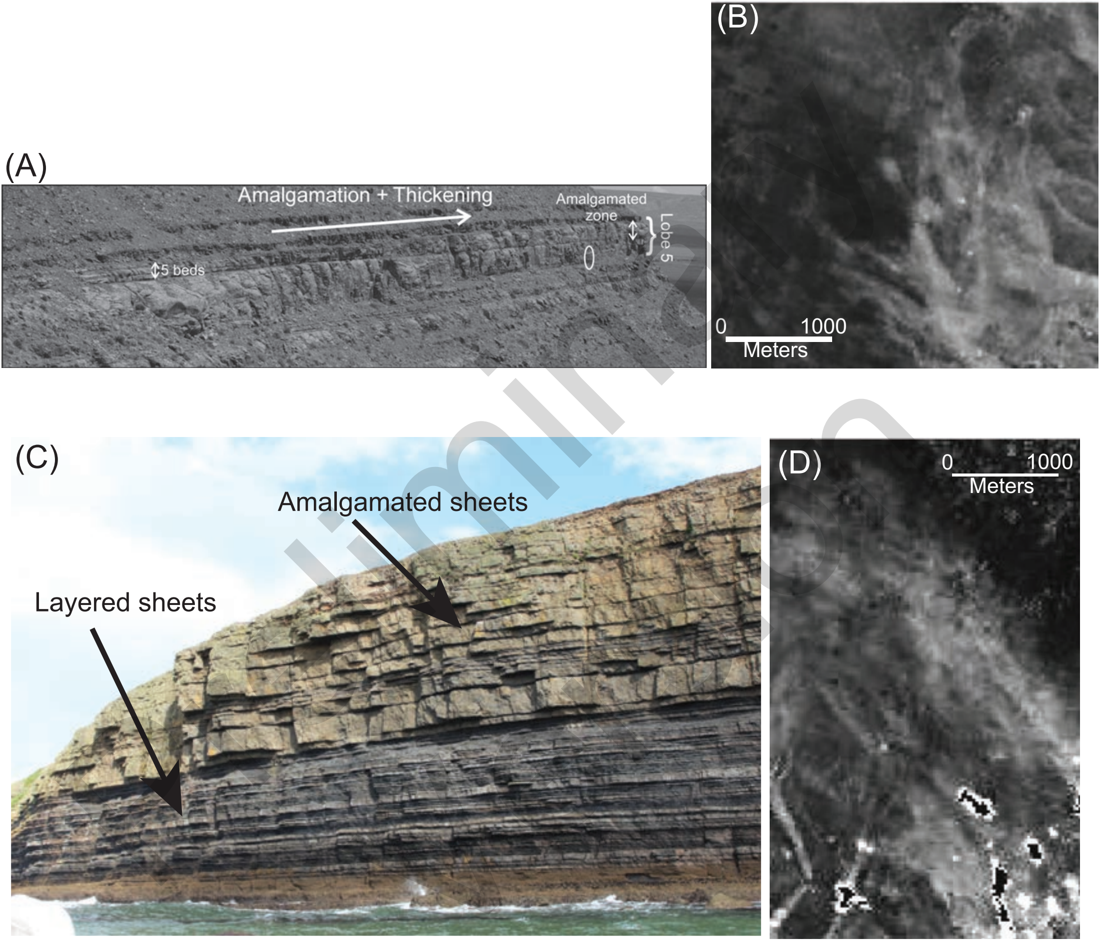

Fig 17 Doughty-Jones et al.